Available online at www.sciencedirect.com

SciVerse ScienceDirect

Geochimica et Cosmochimica Acta 99 (2012) 224–242

Geochimica et Cosmochimica Acta

www.elsevier.com/locate/gca

Carbonate clumped isotope variability in shallow water corals: Temperature dependence and growth-related vital effects

Casey Saenger [a,*], Hagit P. Affek [a], Thomas Felis [b], Nivedita Thiagarajan [c], Janice M. Lough [d], Michael Holcomb [e]

[a] Department of Geology and Geophysics, Yale University, New Haven, CT 06520, USA
[b] MARUM—Center for Marine Environmental Sciences, University of Bremen, 28359 Bremen, Germany
[c] Division of Geological and Planetary Sciences, California Institute of Technology, Pasadena, CA 91125, USA
[d] Australian Institute of Marine Science, PMB 3, Townsville MC, Queensland 4810, Australia
[e] University of Western Australia, Crawley, WA 6009, Australia

Received 2 May 2012; accepted in revised form 19 September 2012; available online 28 September 2012

Abstract

Geochemical variations in shallow water corals provide a valuable archive of paleoclimatic information. However, biological effects can complicate the interpretation of these proxies, forcing their application to rely on empirical calibrations. Carbonate clumped isotope thermometry (Δ_{47}) is a novel paleotemperature proxy based on the temperature dependent "clumping" of ^{13}C–^{18}O bonds. Similar Δ_{47}-temperature relationships in inorganically precipitated calcite and a suite of biogenic carbonates provide evidence that carbonate clumped isotope variability may record absolute temperature without a biological influence. However, large departures from expected values in the winter growth of a hermatypic coral provided early evidence for possible Δ_{47} vital effects. Here, we present the first systematic survey of Δ_{47} in shallow water corals. Sub-annual Red Sea Δ_{47} in two *Porites* corals shows a temperature dependence similar to inorganic precipitation experiments, but with a systematic offset toward higher Δ_{47} values that consistently underestimate temperature by ~8 °C. Additional analyses of *Porites*, *Siderastrea*, *Astrangia* and *Caryophyllia* corals argue against a number of potential mechanisms as the leading cause for this apparent Δ_{47} vital effect including: salinity, organic matter contamination, alteration during sampling, the presence or absence of symbionts, and interlaboratory differences in analytical protocols. However, intra- and inter-coral comparisons suggest that the deviation from expected Δ_{47} increases with calcification rate. Theoretical calculations suggest this apparent link with calcification rate is inconsistent with pH-dependent changes in dissolved inorganic carbon speciation and with kinetic effects associated with CO_2 diffusion into the calcifying space. However, the link with calcification rate may be related to fractionation during the hydration/hydroxylation of CO_2 within the calcifying space. Although the vital effects we describe will complicate the interpretation of Δ_{47} as a paleothermometer in shallow water corals, it may still be a valuable paleoclimate proxy, particularly when applied as part of a multi-proxy approach.

1. INTRODUCTION

Variations in the oxygen isotopic composition ($\delta^{18}O$) of biogenic carbonates have long been recognized as a valuable proxy for past ocean temperature (McCrea, 1950; Urey et al., 1951; Epstein et al., 1953; Emiliani, 1955), when changes in seawater $\delta^{18}O$ are accounted for (e.g. Shackleton, 1967). In corals, Weber and Woodhead (1972) and Weber (1973) demonstrated a temperature dependence of $\delta^{18}O$ in both hermatypic (reef building) and ahermatypic scleractinian corals. These seminal works provided the foundation for the paleoclimatic application of coral $\delta^{18}O$, including multi-century records of tropical climate variability (e.g. Cole et al., 1993; Linsley et al., 1994; Quinn et al., 1998; Felis

* Corresponding author.
E-mail address: casey.saenger@yale.edu (C. Saenger).

0016-7037/$ - see front matter © 2012 Elsevier Ltd. All rights reserved.
http://dx.doi.org/10.1016/j.gca.2012.09.035

et al., 2000) and reconstructions of abrupt changes in ocean circulation (Smith et al., 1997).

In spite of its temperature dependence, Weber and Woodhead (1972) and Weber (1973) showed that the $\delta^{18}O$ of coral aragonite was not in isotopic equilibrium with the surrounding seawater, but rather had lower $^{18}O/^{16}O$ ratios than predicted by the Epstein et al. (1953) paleotemperature scale. Evidence that $\delta^{18}O$ decreases with increasing photosynthetic activity of a coral's symbiotic algae (Erez, 1978) suggests a degree of biological influence on isotopic disequilibrium. These biogenic vital effects prevent a simple interpretation of $\delta^{18}O$ and other geochemical proxies solely in terms of temperature. For example, $\delta^{18}O$-temperature calibrations differ significantly among conspecific corals, even at the same site, and they are rarely stable through time (Lough, 2004; Grottoli and Eakin, 2007). In addition, $\delta^{18}O$ varies among contemporaneous fast and slow growing skeletal regions deposited under identical environmental conditions in a single coral (Land et al., 1975; McConnaughey, 1989a,b) and among fast and slow growing corals from the same reef site (Felis et al., 2003). Finally, distinct $\delta^{18}O$ differences have been observed in coral microstructures, with centers of calcification having lower and more stable values, while adjacent fibers show higher and more scattered values (Julliet-Leclerc et al., 2009).

Considerable evidence that coral $\delta^{18}O$ is influenced by factors other than temperature and the oxygen isotope composition of seawater make it desirable to develop new coral-based paleotemperature proxies that either avoid or account for vital effects. Carbonate clumped isotope thermometry is a novel tool for reconstructing past temperature variability that may be insensitive to the vital effects that influence $\delta^{18}O$ (Eiler, 2011). Based on the thermodynamic preference for ^{13}C–^{18}O bonds in the crystal lattice at lower temperatures, carbonate clumped isotope thermometry constrains temperature from the carbonate phase alone (Schauble et al., 2006; Ghosh et al., 2006; Eiler, 2011), independent of the carbon and oxygen isotopic composition of the calcifying fluid from which it precipitates. Isotopic "clumping" is measured via analyses of $^{13}C^{18}O^{16}O$ in CO_2 produced through the acid digestion of carbonate samples and is reported as Δ_{47}, the permil enrichment in $^{13}C^{18}O^{16}O$ relative to the stochastic distribution of heavy isotopes among all possible isotopologues (Eiler and Schauble, 2004; Wang et al., 2004; Ghosh et al., 2006). Based on inorganic calcite precipitated at 1–50 °C, a calibration of Δ_{47} vs. temperature (Ghosh et al., 2006) generally agrees with a diverse suite of biogenic aragonites and calcites (Came et al., 2007; Tripati et al., 2010; Zaarur et al., 2011; Thiagarajan et al., 2011; Eiler, 2011), supporting the possibility that the proxy is not subject to biological vital effects.

Previously published measurements of Δ_{47} in bulk coral samples generally agree with inorganic Δ_{47} calibrations (Ghosh et al., 2006). In hermatypic corals, Δ_{47}-based temperatures from Indonesian and northern Red Sea *Porites* corals are within 1.5 °C of their estimated growth temperatures (Ghosh et al., 2006; Thiagarajan et al., 2011). Similar agreement has been demonstrated in ahermatypic deep-sea corals including *Desmophyllum*, *Ennalopsammia* and *Caryophyllia* species (Thiagarajan et al., 2011). However, the only sub-annually resolved coral Δ_{47} data span a single annual cycle in a *Porites* from the northern Red Sea (Ghosh et al., 2006). These data show a clear annual cycle, but with a large amplitude that implies winter seawater temperatures below 0 °C – significantly cooler than the ~21 °C observed (Genin et al., 1995; Felis et al., 2004), and far too cold to support the growth of massive *Porites* corals. Furthermore, the Δ_{47}-temperature relationship implied by these data is much steeper than that observed in other biogenic carbonates and inorganic calibrations (Ghosh et al., 2006; Dennis and Schrag, 2010; Eiler, 2011) suggesting non-equilibrium Δ_{47} isotope effects. Processes associated with coral $\delta^{18}O$ vital effects such as growth rate, hydration/hydroxylation kinetics, calcifying fluid pH and photosynthetic activity may explain the large amplitude of sub-annual Δ_{47} variability, but these mechanisms have yet to be thoroughly investigated with respect to Δ_{47} in shallow water corals. In addition, evidence that oxygen isotope fractionation is influenced by salinity (Zeebe, 2007) suggests that the high salinity of the Red Sea could also affect Δ_{47}. Finally, we note that the pioneering work of Ghosh et al., (2006) was conducted in the early days of carbonate clumped isotope paleothermometry and the anomalous sub-annual behavior observed in corals may result, in part, from uncertainties associated with the analytical protocols and low levels of replication that were standard practice at that time.

Here, we present an assessment of carbonate clumped isotope variability in shallow water corals. We discuss data from a suite of symbiotic/asymbiotic and hermatypic/ahermatypic corals from the Red Sea, Pacific, and Atlantic Oceans, including sub-annual measurements of the same Red Sea coral discussed in Ghosh et al. (2006) and an additional *Porites* from the region. We examine the changes in Δ_{47} associated with processes capable of producing vital effects in an effort to better understand carbonate clumped isotope variability in shallow water corals.

2. MATERIALS AND METHODS

2.1. Coral samples and environmental records

We analyzed two northern Red Sea *Porites* corals at sub-annual resolution. BRI-1, the coral measured previously by Ghosh et al. (2006), was collected in 1995 from a water depth of ~5 m within Ras Muhammad National Park (Table 1). Approximately 200 km to the north, *Porites* coral EILAT-15B was collected at ~15 m water depth in the northern Gulf of Aqaba (Felis et al., 2003). *In situ* sea surface temperature (SST) near EILAT-15B varies annually by ~5 °C, from 21.1 ± 0.4 °C to 26.3 ± 0.6 °C (1988–1995; Genin et al., 1995). Equivalent *in situ* data is not available for BRI-1, but 1° × 1°, satellite-derived SSTs indicate a ~7 °C range from 20.7 ± 0.7 °C to 27.9 ± 0.5 °C (1982–2008; Reynolds et al., 2002). We note that these satellite-derived data may overestimate the amplitude of the local seasonal SST cycle near BRI-1, as is observed near EILAT-15B (Genin et al., 1995; Felis et al., 2004). Salinity at both Red Sea sites is higher than typical seawater with an estimated annual mean of 40.8 ± 0.1 psu (Carton and Giese, 2008).

Table 1
Location and environmental conditions of coral samples.

Sample	Location	Latitude	Longitude	Genus	Depth (m)	Symbiotic	T (°C)
EILAT-15B	Red Sea, Israel	29° 30.2′ N	34° 55.2′ E	*Porites*	15	Y	21.1-26.3[a]
BRI-1	Red Sea, Egypt	27° 50.9′ N	34°18.6′ E	*Porites*	5	Y	20.1-27.9[b]
RIB-B54	GBR, Australia	18° 28.8′ S	146° 52.8′ E	*Porites*	4	Y	26.3[c]
21-141-B11	GBR, Australia	21° 31.2′ S	151° 13.2′ E	*Porites*	4	Y	25.2[c]
BAH-SID	Bahamas	25° 50.3′ N	78° 37.2′ W	*Siderastrea*	5	Y	27.1[b]
AST-H59	Woods Hole, USA	41° 31.7′ N	70° 40.4′ W	*Astrangia*	5	Y	14.6[d]
AST-E1	Woods Hole, USA	41° 31.7′ N	70° 40.4′ W	*Astrangia*	5	Y	14.6[d]
AST-AZ	Woods Hole, USA	41° 31.7′ N	70° 40.4′ W	*Astrangia*	5	N	14.6[d]
45923	North Atlantic	7° 24.0′ N	56° 18.0 ‘W	*Caryophyllia*	1318	N	4.6[e]

[a] Genin et al. (1995).
[b] Integrated Global Ocean Services System (IGOSS). Reynolds et al. (2002).
[c] In situ mean (1996–2007) at Kelso Reef and (1995–2010) at Turner Reef. (http://data.aims.gov.au/).
[d] In situ annual and April–December mean (1998–2007). http://dlaweb.whoi.edu/DIG_RES/water_temp.php.
[e] From Thiagarajan et al. (2011).

Each coral was sampled at ~1.5 mm intervals along its axis of maximum growth using a micromill at slow speed (~1500 r.p.m.). This approach is distinct from that of Ghosh et al. (2006), who, to the best of our knowledge, sampled off this axis (Electronic Supplement Fig. 1). We milled 11 samples from BRI-1 along the growth axis between 65 and 80 mm from the top of the coral. Using $\delta^{18}O$ in all 11 samples as a guide, Δ_{47} was analyzed at only six intervals near seasonal $\delta^{18}O$ maxima and minima. We milled an additional bulk sample across a ~1 cm region along the growth axis adjacent to the bulk sample of Thiagarajan et al. (2011) (Electronic Supplement Fig. 1).

Although it has been argued that the growth temperature of Ghosh et al.'s (2006) data cannot be confidently constrained (e.g. Eiler, 2011), an accurate age model can be constructed from other geochemical signals and directly compared to observed SST if certain assumptions are made. Our age model for BRI-1 is based on the seasonal Sr/Ca and $\delta^{18}O$ data plotted versus distance by Ghosh et al. (2006) (Fig. 6 therein) and assumes that the distance equal to 0 approximates the coral's July, 1995 collection date. From this date, four Sr/Ca and $\delta^{18}O$ minima occur between 10 and 60 mm, which we interpret as the summers of 1991–1994. This indicates the Δ_{47} minima of Ghosh et al. (2006) represent the summers of 1989 (~84 mm) and 1990 (~66 mm), and their Δ_{47} maximum represents the winter of 1990 (~75 mm). We assign the dates of warmest (coldest) SST to BRI-1 $\delta^{18}O$ minima (maxima) and linearly interpolate between them. The possibility that this age model assigns incorrect dates to maxima and minima will not significantly impact our assigned temperatures considering seasonal SST extremes vary by <0.7 °C between 1988 and 1995 (1σ s.d.; Genin et al., 1995; Reynolds et al., 2002). Assuming our BRI-1 ages are correct, we sampled EILAT-15B to overlap in time using previously assigned dates (Felis et al., 2004).

Analyses from a Great Barrier Reef (GBR), Australia *Porites* coral were used to assess the potential effects of salinity, organic matter contamination, and sampling method on Δ_{47} variability. Coral RIB-B54 was collected in the year 2000 at a water depth of ~4 m (Table 1). Mean annual SST, measured *in situ* at nearby Kelso Reef, is 26.3 ± 0.4 °C, with a seasonal maximum of 28.9 ± 1.0 °C in February and a minimum of 23.4 ± 0.6 °C in August (http://data.aims.gov.au/). Reanalysis data suggests an annual mean salinity of 35.2 ± 0.1 (Carton and Giese, 2008). Our initial sampling of RIB-B54 milled ~20 mg of skeleton across a ~1 cm track below the coral tissue layer that represents ~1 year of growth along the coral's axis of maximum extension (Electronic Supplement Fig. 2). To assess the potential impact of organic matter contamination, we milled a second ~40 mg bulk sample from the tissue layer immediately above our initial sampling (Electronic Supplement Fig. 2). This tissue-bearing sample was split into two ~20 mg aliquots. The first aliquot was sonicated in 10% (v/v) ultra-pure H_2O_2 (SEASTAR Chemicals Baseline) for 4 h at room temperature and then allowed to dry completely in a vacuum oven also at room temperature. The complementary aliquot was left untreated. Finally, to examine if ^{13}C–^{18}O "clumping" is altered by frictional heating during milling, a third set of samples was collected by breaking a ~1 cm^3 block from RIB-B54. A bulk sample of ~20 mg was micro-milled from the block along its plane of upward extension. The remainder of the block, representing a nearly identical time period, was then ground using a mortar and pestle.

To assess the effect of calcification rate on Δ_{47} we sampled a second GBR *Porites*, coral B11, which was collected at 21-141 Reef in May, 1989 from a water depth of ~4 m (Table 1). Annual *in situ* SST at nearby Turner Reef averages 25.2 ± 0.7 °C. Using annual density banding as a guide, four ~20 mg samples were milled along an "isochron" of variable extension rates that represents growth during the years 1967–1969 (Fig. 1). Samples span a gradient of extension rates from 8.1 mm yr^{-1} along the coral's axis of maximum growth to 2.3 mm yr^{-1} along its side.

We then evaluated the possibility of species-specific Δ_{47} effects by analyzing a slow growing (~2.5 mm yr^{-1}) hermatypic *Siderastrea* spp. coral (Saenger et al., 2009) (Table 1). BAH-SID was collected from the northern edge of the Great Bahama Bank in 1991 at a water depth of ~5 m. We estimate annual mean SST and salinity at the site to

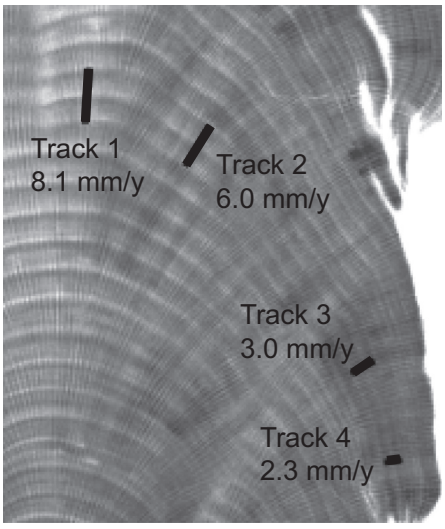

Fig. 1. X-radiograph of Great Barrier Reef *Porites* 21-141-B11 (see Table 1) showing annual density banding. Four samples, each representing a 2 year isochron, were milled at extension rates of 2.3–8.1 mm yr^{-1}.

be 27.1 ± 0.2 °C and 36.4 ± 0.1, respectively (Reynolds et al., 2002; Carton and Giese, 2008). Approximately 20 mg of powder milled from a ~1 cm long channel along the axis of maximum growth likely represents ~5 years during the 1980s.

The influence of photosynthetic symbionts was assessed using zooxanthellate and azooxanthellate *Astrangia* species corals from the subtropical North Atlantic (Holcomb et al., 2010; Table 1). Three *Astrangia* corals were collected in Woods Hole, Massachusetts, USA from a depth of ~5 m in 2009. Of these, samples AST-E1 and AST-H59 possessed symbiotic zooxanthellae, while sample AST-AZ was azooxanthellate. After bisecting colonies with a diamond saw, ~100 mg bulk samples were milled from below the coral's tissue layer. Because *in situ* monitoring of *Astrangia* corals indicates that growth occurs only during the warm season (Dimond and Carrington, 2007), we estimate the growth temperature of these specimens to be the April–December mean (14.6 ± 0.6 °C) of *in situ* data (http://dla-web.whoi.edu/DIG_RES/water_temp.php).

Finally, to establish a cold water end member, we re-measured a deep-sea coral at Yale University that was discussed previously by Thiagarajan et al. (2011). *Caryophyllia* coral sample 45923, which is ahermatypic and azooxanthellate, derives from a depth of 1318 m in the tropical North Atlantic (Table 1), where temperatures are effectively constant at 4.6 °C.

2.2. Analytical protocol

Sample analysis generally followed the protocol described by Zaarur et al. (2011). In brief, 4–5 mg of aragonite coral powder was digested overnight in 105% phosphoric acid at 25 °C for a minimum of 8 h. Resulting CO_2 was extracted cryogenically and purified of potential hydrocarbon contaminants by passing it through a gas chromatograph column (Supelco Q-Plot, 30 m length, 0.53 mm ID) at −20 °C. Clean CO_2 was measured using a Finnigan MAT-253 gas source isotope ratio mass spectrometer configured to measure masses 44 through 49 at the Yale University Earth Systems Center for Stable Isotopic Studies. The mass 47 beam is composed primarily of $^{13}C^{16}O^{18}O$, and is used to calculate R^{47}, the ratio of mass 47 to mass 44. Δ_{47} is then calculated relative to the stochastic distribution of isotopologues (Wang et al., 2004; Huntington et al., 2009):

$$\Delta_{47} = ((R^{47}_{measured}/R^{47}_{stochastic} - 1) - (R^{46}_{measured}/R^{46}_{stochastic} - 1) - (R^{45}_{measured}/R^{45}_{stochastic} - 1)) \times 1000$$

The mass 48 and 49 beams are measured to screen for contamination from hydrocarbons. Each CO_2 measurement consisted of 90 sample-standard cycles at a 20 s ion integration time. All samples were fully replicated (i.e. replicate CO_2 extractions from a fresh aliquot of the same powder) at least three times, which we consider to be the minimum for reliable Δ_{47} results. An aragonite acid digestion fractionation factor of 10.63‰ was applied to oxygen isotope data (Kim et al., 2007a), and both $\delta^{18}O$ and $\delta^{13}C$ are reported using the VPDB scale.

Although this protocol is similar to that of Ghosh et al. (2006), it differs from the current method used at the California Institute of Technology (Caltech). Phosphoric acid digestion at Caltech is conducted at 90 °C using an automated system and Δ_{47} values are corrected by 0.081‰ relative to the value expected for a 25 °C reaction to account for a temperature dependent fractionation in the digestion reaction (Passey et al., 2010). To evaluate the possibility of interlaboratory differences, samples from each lab were exchanged. Sample 45923, prepared and previously measured at Caltech (Thiagarajan et al., 2011), was re-measured at Yale while RIB-B54 and AST-H59 were also analyzed at Caltech.

Tables 2–4 present Δ_{47} results in the traditional reference frame, while results in the absolute reference frame developed by Dennis et al. (2011) are provided in Electronic Supplement Tables 1–3. Temperature estimates are based on the inorganic calibration of Ghosh et al. (2006). We note that this calibration differs significantly from the Δ_{47}-temperature relationship of Dennis and Schrag (2010) and possible explanations for discrepant calibrations are discussed elsewhere (e.g. Eiler, 2011). Although this topic is clearly an important issue that requires further research, the general conformity of most biogenic carbonates to the Ghosh et al. (2006) calibration relationship makes it the relevant reference point.

3. RESULTS AND DISCUSSION

3.1. Δ_{47} in Red Sea *Porites*

Sub-annual data for EILAT-15B and BRI-1 are shown in Fig. 2a and b and Table 2. Both corals show clear seasonal cycles in $\delta^{18}O$ and Δ_{47} that are generally in phase (Fig. 2). BRI-1 Δ_{47} variability shows a seasonal amplitude of ~0.03‰, which ranges from 0.704 ± 0.011‰ (1 s.e.) to 0.670 ± 0.009‰. EI-

Table 2
Sub-annual Red Sea *Porites* geochemical data.

Sample	Year	Δ_{47} (‰)	s.e.	$\delta^{18}O$ (‰) VPDB	s.e.	$\delta^{13}C$ (‰) VPDB	s.e.	*n*	SST (°C)[a]	Predicted Δ_{47} (‰)
EILAT-15B										
48	1990.25	0.711	0.007	2.51	0.04	−2.15	0.05	3	20.9	0.665
49	1990.13	0.706	0.014	−2.20	0.05	−2.49	0.04	3	20.9	0.665
50	1990.00	0.698	0.008	−2.68	0.01	−2.95	0.04	3	22.0	0.660
51	1989.88	0.703	0.013	−2.90	0.00	−2.86	0.05	3	23.6	0.652
52	1989.75	0.692	0.005	−2.97	0.02	−3.24	0.03	4	24.8	0.647
53	1989.63	0.681	0.021	−2.90	0.02	−2.85	0.05	4	25.4	0.644
54	1989.50	0.684	0.003	−2.77	0.02	−3.01	0.04	3	23.8	0.651
55	1989.38	0.688	0.008	−2.72	0.05	−2.69	0.04	3	23.2	0.654
56	1989.25	0.682	0.011	−2.64	0.07	−2.61	0.02	4	21.3	0.663
57	1989.13	0.701	0.014	−2.29	0.02	−2.62	0.02	3	20.6	0.666
58	1989.02	0.713	0.009	−2.33	0.03	−3.06	0.01	4	21.5	0.662
59	1988.92	0.698	0.007	−2.56	0.02	−3.36	0.02	3	22.7	0.656
60	1988.82	0.677	0.009	−2.91	0.02	−2.89	0.04	4	23.9	0.651
61	1988.72	0.689	0.009	−3.15	0.02	−2.53	0.04	4	25.5	0.644
62	1988.62	0.671	0.010	−3.26	0.04	−2.75	0.04	3	26.6	0.639
BRI-1										
1	1990.63	0.670	0.009	−3.68	0.03	−0.78	0.01	3	27.97	0.633
2	1990.55	0.682	0.013	−3.65	0.04	−0.97	0.01	3	27.23	0.636
3	1990.46	–	–	−3.46	–	−0.86	–	1	25.07	–
4	1990.38	–	–	−3.28	–	−1.26	–	1	23.85	–
5	1990.30	–	–	−3.01	–	−1.27	–	1	22.33	–
6	1990.21	0.698	0.015	−2.91	0.06	−1.43	0.04	3	21.29	0.663
7	1990.13	0.689	0.011	−2.80	0.02	−1.48	0.10	3	21.01	0.664
8	1990.05	0.704	0.011	−3.07	0.03	−1.62	0.06	3	22.20	0.659
9	1989.96	–	–	−3.31	–	−1.59	–	1	23.42	–
10	1989.88	–	–	−3.58	–	−1.24	–	1	24.50	–
11	1989.80	0.670	0.013	−3.65	0.04	−0.85	0.13	3	27.01	0.637

[a] EILAT-15B SST from Genin et al. (1995), BRI-1 SST from Reynolds et al. (2002).

Table 3
Geochemical results from bulk-sampled coral data.

Sample	Method[a]	Lab[b]	Δ_{47} (‰)	s.e.	$\delta^{18}O$ (‰) VPDB	s.e.	$\delta^{13}C$ (‰) VPDB	s.e.	*n*	*T* (°C)	Predicted Δ_{47} (‰)
BRI-1	mill	Y	0.690	0.008	−3.42	0.10	−0.90	0.07	4	25.2	0.645
RIB-B54	mill	Y	0.686	0.011	−4.76	0.12	−2.84	0.02	4	26.3	0.640
RIB-B54	M + P	Y	0.681	0.002	−4.80	0.07	−2.77	0.07	3	26.3	0.640
RIB-B54 (tissue)	mill	Y	0.678	0.007	−5.19	0.02	−3.35	0.01	3	26.3	0.640
RIB-B54 (H_2O_2)	mill	Y	0.701	0.015	−4.74	0.03	−3.31	0.03	3	26.3	0.640
BAH-SID	mill	Y	0.680	0.011	−2.96	0.05	−0.60	0.12	6	26.8	0.638
AST-H59	M + P	Y	0.700	0.010	−3.54	0.04	−6.46	0.04	3	14.6	0.695
AST-E1	M + P	Y	0.690	0.004	−4.01	0.05	−7.81	0.02	3	14.6	0.695
AST-AZ2	M + P	Y	0.701	0.008	−2.90	0.00	−6.13	0.08	3	14.6	0.695
45923	M + P	Y	0.731	0.006	3.80	0.06	0.80	0.18	11	4.6	0.747
RIB-B54	M + P	C	0.671	0.006	−4.79	0.02	−2.86	0.01	4	26.3	0.640
AST H59	M + P	C	0.714	0.009	−3.55	0.02	−6.57	0.01	4	14.6	0.695
BRI-1[c]	M + P	C	0.638	0.008	−3.68	0.03	−1.16	0.02	4	25.2	0.645
45923[c]	M + P	C	0.744	–	3.14	–	0.29	–	1	4.6	0.747

[a] 'mill' denotes micromilling. 'M + P' denotes mortar and pestle.
[b] 'Y' denotes Yale University. 'C' denotes California Institute of Technology.
[c] Data from Thiagarajan et al. (2011).

LAT-15B shows similar seasonal Δ_{47} variability that ranges from 0.713 ± 0.009‰ to 0.671 ± 0.010‰. Using the calibration of Ghosh et al. (2006), the Δ_{47} amplitude we observe predicts a seasonal temperature amplitude of 6–7 °C, which is similar to the ~5–7 °C observed. Furthermore, regressing SST ($10^6 \times T^{-2}$) versus sub-annual BRI-1 and EILAT-15B Δ_{47} results in slopes that are nearly parallel to inorganic calibrations, indicating that the corals analyzed here have similar temperature sensitivities to the abiogenic calcite calibration (Fig. 3). However, both corals deviate from the predicted Δ_{47} value by an average Δ_{47} offset of +0.038‰ (Fig. 2a and b), which corresponds to temperatures that are

Table 4
Geochemical results from variable growth rate 21-141-B11 isochron.

Track	Extension rate (mm yr^{-1})	Δ_{47} (‰)	s.e.	$\delta^{18}O$ (‰) VPDB	s.e.	$\delta^{13}C$ (‰) VPDB	s.e.	n	Predicted Δ_{47} (‰)
1	8.1	0.687	0.008	−4.77	0.05	−0.73	0.16	3	0.645
2	6.0	0.699	0.012	−4.73	0.03	−0.64	0.08	3	0.645
3	3.1	0.691	0.001	−4.03	0.05	0.05	0.06	3	0.645
4	2.3	0.672	0.007	−3.72	0.02	0.57	0.001	3	0.645

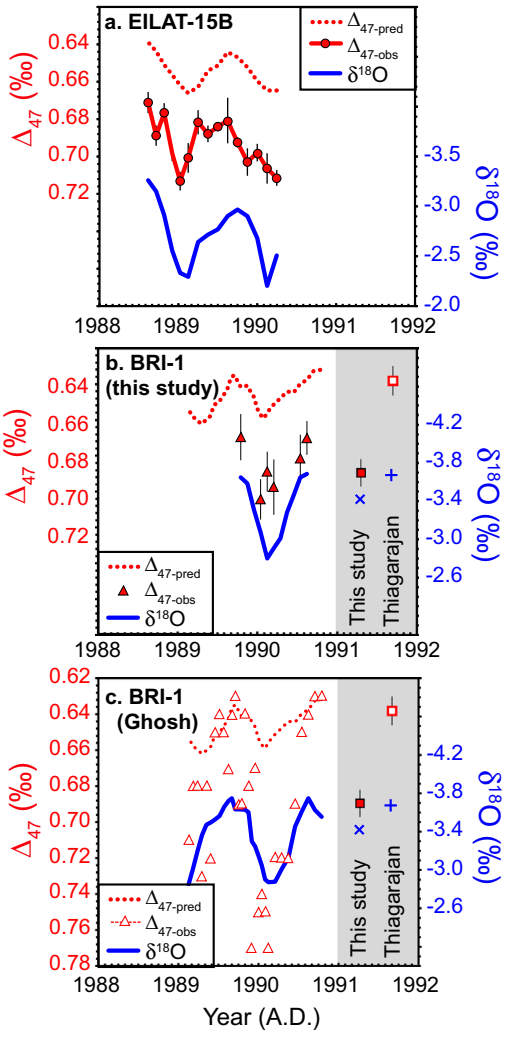

Fig. 2. (a) Sub-annual EILAT-15B Δ_{47} (circles, left axis) and $\delta^{18}O$ (solid line, right axis) compared with the Δ_{47} expected based on *in situ* SST and the Δ_{47}-temperature calibration of Ghosh et al. (2006) (dashed line, left axis). (b) As in (a) for sub-annual BRI-1 Δ_{47} (filled triangles) and $\delta^{18}O$ (solid line). Bulk sampled BRI-1 Δ_{47} (filled square) and $\delta^{18}O$ (ex) from this work and Δ_{47} (open square) and $\delta^{18}O$ (cross) from Thiagarajan et al. (2011) are also shown. (c) As in (b) for BRI-1 Δ_{47} (open triangles) and $\delta^{18}O$ (solid line) data from Ghosh et al. (2006). Error bars represent 1 standard error of at least three replicates. Note that the Ghosh et al. (2006) $\delta^{18}O$ was corrected by 0.38‰ to account for the calcite acid fraction factor of 10.25% used in that study compared to the aragonite acid fractionation used in this study and in Thiagarajan et al. (2011). Please see the online full color version.

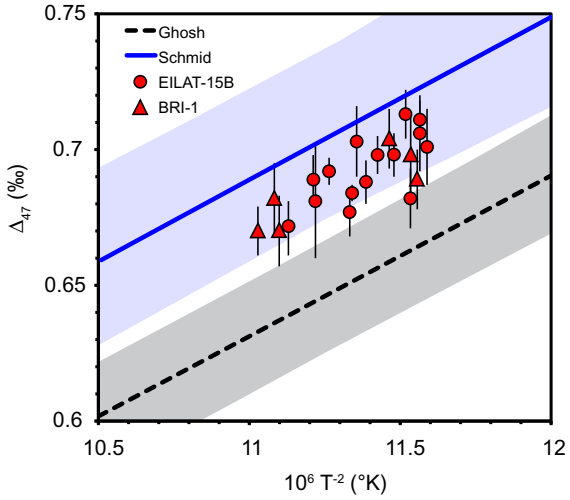

Fig. 3. Δ_{47} versus temperature for sub-annually sampled Red Sea *Porites* corals (symbols) compared with the inorganic precipitation experiments of Ghosh et al. (2006) (black line) and Schmid (2011) (blue line). The experiments of Ghosh et al. (2006) were precipitated slowly at approximately neutral pH to achieve conditions close to isotopic equilibrium while those of Schmid (2011) were precipitated rapidly at pH 9. The slopes of the Ghosh et al. (2006) and Schmid (2011) experiments are $0.0592 \times 10^6\ T^{-2}$ and $0.0599 \times 10^6\ T^{-2}$, respectively. Shaded regions represent 95% confidence intervals. (For interpretation of the references to color in this figure legend, the reader is referred to the web version of this article.)

~8 °C too cool. This apparent vital effect is generally constant throughout the year, with a small tendency toward larger offsets during cool months (Fig. 4a).

Consistent with our sub-annual data, we also find a higher than expected Δ_{47} value in a bulk BRI-1 sample that estimates a temperature ~10 °C cooler than the observed annual mean (Fig. 2b, Table 3). The Δ_{47} value of this bulk sample (0.690 ± 0.008‰) falls within the range of our sub-annual data indicating that the positive Δ_{47} offset cannot be explained by a large sampling bias toward winter values (Fig. 2b). In fact, relative to our sub-annual data, the $\delta^{18}O$ of the bulk BRI-1 sample shows a slight bias toward the warm season suggesting that the reported Δ_{47} offset may be a conservative estimate.

3.1.1. Comparison with previous data

Similar to our sub-annual coral data, the sub-annual BRI-1 Δ_{47} data of Ghosh et al. (2006) show an annual cycle that is in phase with $\delta^{18}O$ (Fig. 2c). However, the amplitude

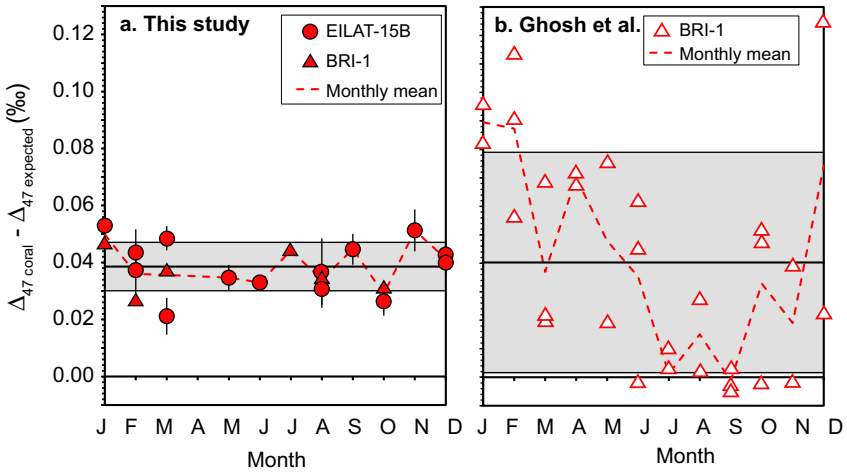

Fig. 4. Offset of measured *Porites* Δ_{47} from the expected value in (a) this study and (b) Ghosh et al. (2006). Values have been binned by month for several years of data. Error bars in (a) are 1 standard error of at least three replicates. The shaded region denotes the 1σ standard deviation of the mean temperature offset.

of this variability is considerably larger (<0.12‰), with a maximum of 0.63‰ and minimum of 0.77‰. These values are equivalent to summer temperatures near 29 °C, winter temperatures of zero, and a seasonal temperature variation of ~30 °C that is far larger than the ~5–7 °C observed. When binned by month, the Δ_{47} data of Ghosh et al. (2006) is close to the expected value from July to September, but shows winter Δ_{47} offsets that are far larger than those observed in our sub-annual data (Fig. 4b). Furthermore, regressing SST ($10^6 \times T^{-2}$) against the sub-annual BRI-1 Δ_{47} data of Ghosh et al. (2006) yields a slope of 0.150‰/($10^6 \times T^{-2}$) that is significantly steeper than the inorganic calibrations (Fig. 3). Although seemingly disparate at first glance, the average Δ_{47} offset of Ghosh et al.'s (2006) data (0.040‰) is nearly identical to the average offset of our sub-annual data. This hints that our record may represent a dampened version of the same signal measured by Ghosh et al. (2006) (Fig. 4). If this is the case, we suggest three possible explanations: (1) sampling resolution (2) analytical noise and/or (3) a growth-related vital effect.

By not replicating Δ_{47} measurements, Ghosh et al. (2006) could sample at a resolution of ~20 samples per year that is double our resolution (~10 samples per year) for triplicate measurements. Lower sampling resolution can underrepresent seasonal extremes, and has been shown to attenuate seasonal $\delta^{18}O$ cycles in hermatypic corals (e.g. Leder et al., 1996). If our lower sampling resolution resulted in a similar effect on Δ_{47}, we would expect the larger amplitude Δ_{47} cycles of Ghosh et al. (2006) to be accompanied by higher amplitude $\delta^{18}O$ variability. To the best of our knowledge, the sub-annual $\delta^{18}O$ data reported by Ghosh et al. (2006) are not the complementary values to their off growth axis-sampled Δ_{47} data, but rather a separate on-axis sampling of BRI-1 (Electronic Supplement Fig. 1). Although this prevents a direct comparison with our data, Ghosh et al.'s (2006) on-axis $\delta^{18}O$ record, which also has a sampling resolution of ~20 samples per year, shows a seasonal $\delta^{18}O$ amplitude that is nearly identical to our data (Fig. 2b and c) and argues against sample aliasing as the primary cause of our lower amplitude signal.

Alternatively, Ghosh et al.'s (2006) Δ_{47} data were generated using mass spectrometric analyses with short counting times (<1000 s) and were not replicated, leading to relatively low precision that may explain the larger amplitude of their seasonal Δ_{47} cycle. The relatively large standard errors of 0.01–0.035‰ in the coral data of Ghosh et al. (2006) can be reduced to 0.005–0.01‰ at long counting times (>3000 s; Thiagarajan et al., 2011) such as those used in this study. Furthermore, the improved precision achieved through replication can reduce external standard error from >0.014‰ for samples replicated fewer than three times to ~0.002‰ for samples measured six times (Thiagarajan et al., 2011). Thus, the larger deviations from a mean Δ_{47} offset of ~0.04‰ in the data of Ghosh et al. (2006) (Fig. 4b) could be caused by the increased analytical noise in that early study. However, we would expect this mechanism to cause similar Δ_{47} offsets during all seasons and it is unclear why it would cause little or no offset during summer and strong positive offsets in winter. In light of this, it seems likely that other mechanisms are at least partially responsible for the high amplitude of Ghosh et al.'s (2006) annual Δ_{47} cycle.

A growth-related vital effect could also cause differences in the seasonal amplitude of BRI-1 Δ_{47}. As mentioned above, the annual Δ_{47} cycles in Ghosh et al. (2006) may have been sampled off the maximum growth axis of BRI-1, while the reported $\delta^{18}O$ values come from a separate sampling along the axis of maximum growth (Electronic Supplement Fig. 1). Evidence that *Porites* $\delta^{18}O$ increases by ~0.25‰ between a maximum growth axis and a parallel minimum growth axis (Cohen and Hart, 1997) suggests the sampling strategy of Ghosh et al. (2006) could lead to unexpected kinetic and/or biological effects. For example, a sampling transect that deviated from a single growth axis could produce an unstable Δ_{47} signal that may explain the large sub-annual Δ_{47} cycles observed by Ghosh et al. (2006). If this is the case, it implies significant macro-scale

heterogeneities within a coral skeleton, which have the potential to overwhelm the temperature signal of interest. The possible impacts of kinetic and/or biological effects are discussed further in section in Section 3.3.3.

The positive Δ_{47} offset we measure in Red Sea *Porites* corals is at odds with the result of Thiagarajan et al. (2011) who report a bulk BRI-1 Δ_{47} value of $0.638 \pm 0.008‰$ that is close to the value predicted by inorganic calibrations (Fig. 2b, Table 3). This well-replicated ($n = 4$) sample was collected adjacent to our bulk BRI-1 sample and should represent a similar time interval (Electronic Supplement Fig. 1). However, the $-3.68 \pm 0.03‰$ bulk $\delta^{18}O$ value reported by Thiagarajan et al. (2011) is closer to the summer $\delta^{18}O$ minimum of sub-annual data than the value $-3.42 \pm 0.1‰$ we measure (Fig. 2b), suggesting it may reflect a sampling bias toward summer growth. If this is the case, it may be more appropriate to compare the BRI-1 Δ_{47} measured by Thiagarajan et al. (2011) to warm season SST rather than mean annual. However, such a seasonal bias is not large enough to explain the entire difference between the two BRI-1 Δ_{47} values considering that even our warm season BRI-1 data shows significantly higher Δ_{47} than the bulk sample of Thiagarajan et al. (2011). Instead, the discrepancies between bulk BRI-1 Δ_{47} data could be an analytical artifact, but as discussed in the following sections neither our analytical protocol nor inter-laboratory differences seem responsible for the discrepant results.

3.2. Validation of a positive Δ_{47} offset

To rule out the possibility that the higher than expected Δ_{47} we observe in Red Sea *Porites* is an analytical artifact, we conducted a series of tests that assessed inter-laboratory differences in sample preparation and measurement. With respect to sampling, Thiagarajan et al. (2011) cut a bulk sample from BRI-1 using a rotary tool and then manually crushed the sample using a mortar and pestle to minimize alteration of ^{13}C–^{18}O clumping. In contrast, we sampled BRI-1 using a slow speed micromill that may alter metastable aragonite through frictional heating. However, our test of micromilling versus manual crushing resulted in nearly identical Δ_{47} in two aliquots of *Porites* RIB-B54 (Table 3). This indicates that slow speed micromilling does not alter ^{13}C–^{18}O clumping by frictional heating, and that the positive Δ_{47} offsets we observe are not a sampling artifact.

It is also possible that the higher Δ_{47} we measure in BRI-1 could be caused by differences in sample preparation. For example, the samples analyzed at Caltech in this study were digested at 90 °C in a common acid bath and the resulting CO_2 was purified using an automated system. In contrast, Yale samples were reacted at 25 °C and purified manually using a vacuum line and gas chromatograph. A critical component of the purification step is the removal of volatile organic molecules that are not separated from CO_2 during cryogenic freezing. If not removed, these organics can break down in the mass spectrometer ion source to produce mass 47 fragments and higher than expected Δ_{47}. Although both laboratory protocols include steps intended to remove these organics, it is possible that one laboratory eliminates certain organic molecules not separated by the other. To test for the presence of recalcitrant organic molecules, we equilibrated CO_2 extracted from BRI-1 with water for more than 24 h at 25 °C. The Δ_{47} value for CO_2–H_2O equilibrated at 25 °C is well constrained over a given time period, and was $0.864 \pm 0.014‰$ (s.e.; $n = 4$) for the 3 months surrounding our analysis of the BRI-1 sample. If BRI-1 was contaminated, we would expect coral-derived CO_2 equilibrated with water to be significantly higher than $0.864 \pm 0.014‰$, while we would expect BRI-1 to have a similar value if no organic contaminants are present. We measure a Δ_{47} value of $0.879 \pm 0.027‰$ ($n = 1$; 1 s.d. of 9 acquisitions) in CO_2 extracted from BRI-1 and equilibrated with water, which is statistically identical to the expected value. This strongly suggests that the Yale method effectively removes volatile organic molecules and that these contaminants are not the source of positive Δ_{47} offsets.

Because removing organic matter using a 1% H_2O_2 treatment has been shown to increase the precision of foraminiferal Δ_{47} measurements (Tripati et al., 2010) we also tested if pretreatment affected coral Δ_{47}. Although total organic carbon in coral skeleton is <0.05 wt.% (Ingalls et al., 2003), the possibility that the samples we measure contain organic matter not present in the aliquot analyzed by Thiagarajan et al. (2011) cannot be ruled out *a priori*. We tested this possibility by measuring low organic carbon bulk skeleton and high organic carbon tissue-bearing skeleton in *Porites* RIB-B54. Results show that both samples have Δ_{47} values that are within error of each other (Table 3), albeit still higher than the value predicted by the Ghosh et al. (2006) inorganic calibration. This further suggests that our sample preparation method effectively removes organic matter, and that potential contamination is not the primary cause of positive Δ_{47} offsets. Furthermore, treatment of tissue-bearing skeleton with H_2O_2 does not reduce Δ_{47}, but rather increases it slightly (Table 3), providing additional evidence that organic matter is not the source of positive Δ_{47} offsets. Although our H_2O_2 treatment is harsher than that used previously (e.g. Tripati et al., 2010), it suggests that such pretreatment could alter ^{13}C–^{18}O clumping in corals either through partial isotopic exchange or minor dissolution and should be used cautiously.

As a final confirmation that analytical differences between the two laboratories are not responsible for higher than expected Δ_{47}, aliquots from the same bulk powder of three coral samples (RIB-B54, AST-H59 and 45923) were measured independently at both Yale and Caltech. Results show that Δ_{47} values between the two laboratories are generally within error and exhibit no consistent offset (Table 3). Furthermore, RIB-B54 Δ_{47} values measured at Yale and Caltech both display positive Δ_{47} offsets, while the Δ_{47} of AST-H59 and 45923 are closer to the expected value. This inter-laboratory comparison argues against an analytical source for the Δ_{47} offset we measure between many corals and the abiogenic calibration of Ghosh et al. (2006).

The disagreement between our BRI-1 Δ_{47} and that of Thiagarajan et al. (2011) remains an important, but unresolved, issue that deserves further work. If both BRI-1 values are valid, their disagreement raises the possibility that macroscale Δ_{47} heterogeneities may occur in nearly coeval portions of *Porites* coral skeletons, and may be as large

as the temperature signal of interest. Until a systematic study of intra-coral Δ_{47} heterogeneity can be performed however, the rigorous replication and thorough screening of our data support its reliability. In the absence of additional information, we conclude that the positive Δ_{47} offsets we observe are the result of environmental, biologic and/or kinetic processes that cause non-temperature-dependent Δ_{47} variability.

3.3. Potential sources of high Δ_{47}

Although an empirical calibration could be constructed from our sub-annual *Porites* data to correct for its offset from established temperature calibrations, this approach cannot be considered rigorous unless the mechanism(s) underlying non-equilibrium Δ_{47} variability are understood. A mechanistic understanding of Δ_{47} deviations from apparent equilibrium is aided by decades of work on oxygen isotope fractionation, which demonstrate that $\delta^{18}O$ is affected by a number of factors other than temperature. We consider these processes to be candidate mechanisms for the high Δ_{47} values observed in Red Sea *Porites* and we evaluate their influence in the following sections.

3.3.1. Salinity

Net evaporation of $\sim$200 cm yr^{-1} in the semi-enclosed Red Sea (Morcos, 1970; Ahmad and Sultan, 1989) leads to salinity above 40 psu (Carton and Giese, 2008) that is markedly higher than that of the open ocean ($\sim$35 psu). Although some inorganic precipitation experiments find no significant change in oxygen isotope fractionation factor (α) with ionic strength (e.g. Tarutani et al., 1969; Kim et al. 2007b), other work suggests a subtle effect. For example, Li et al. (1997) found α to linearly decrease by $\sim$0.13‰ psu^{-1} in inorganic carbonates precipitated across a wide range of salinity and temperature (8.4–84.1 psu, 0–37 °C). Theoretical calculations predict a similar dependence and estimate that α between dissolved inorganic carbon (DIC) and water (25 °C; pH 8.2) is 0.14‰ lower at 41 psu than at 35 psu (Zeebe, 2007). Although the influence of salinity may be reduced at fast precipitation rates Zeebe (2007) suggests that it increases at high pH and may be pronounced in a coral's calcifying space (pH 8.5–9.0; Al-Horani et al., 2003; Venn et al., 2011) with α being 0.20–0.25‰ lower at 41 psu than at 35 psu.

The influence of salinity on $\delta^{18}O$ raises the possibility that high Red Sea salinity causes the positive Δ_{47} offsets in BRI-1 and EILAT-15B, in which case we would expect offsets to be smaller or absent in other *Porites* from sites with typical marine salinity. We tested this by measuring Δ_{47} in *Porites* RIB-B54 from the Great Barrier Reef (salinity $= 35.2 \pm 0.1$ psu; Carton and Giese, 2008). Results show RIB-B54 also displays high Δ_{47} that is similar to Red Sea *Porites* values (Table 3), ruling out a detectable salinity effect on Δ_{47}.

3.3.2. Mineralogy

The oxygen isotopic fractionation between aragonite and water is known to be larger than that for calcite (Kim et al., 2007a), suggesting that mineralogy may potentially affect Δ_{47} as well. Indeed, theoretical calculations suggest that kinetic effects during phosphoric acid digestion may cause aragonite Δ_{47} to be $\sim$0.015‰ higher than calcite at a given temperature (Guo et al., 2009). This prediction has the same sign as the Δ_{47} offsets in shallow water aragonitic corals, but its magnitude is far smaller than the $\sim$0.04‰ we measure, suggesting that mineralogy is not the primary cause of Δ_{47} offsets. Furthermore, Δ_{47} values of many biogenic aragonites, including the deep sea corals in this study, generally agree with Ghosh et al.'s calcite calibration (Came et al., 2007; Thiagarajan et al., 2011), while aragonitic otoliths hint at a potential negative Δ_{47} offset (Ghosh et al., 2007). These data argue against a systematic mineralogical bias in the Δ_{47} of carbonates.

3.3.3. Kinetic and biologic vital effects

The tests discussed above, as well as the general agreement between the abiogenic calibrations and biogenic calcites and aragonites other than shallow water corals, suggest that temperature is the primary environmental variable controlling Δ_{47} (Eiler, 2011). If environmental variables other than temperature do not affect Δ_{47}, then kinetic and/or biologic vital effects may be responsible for the higher than expected Δ_{47} we observe. Shallow water corals are among the fastest marine calcifyers, and this rapid growth is intimately linked with the presence of symbiotic zooxanthellate (e.g. Goreau, 1959). Periods of active photosynthesis show large increases in calcification (Barnes and Chalker, 1990) and facultatively symbiotic corals show increased calcification when zooxanthellae are present (Jacques and Pilson, 1980). Both field and laboratory studies indicate that enhanced photosynthesis is associated with lower coral $\delta^{18}O$ (Erez, 1978; Omata et al., 2008) suggesting that it may also affect Δ_{47}. Consistent with this work, we find symbiont-bearing *Astrangia* corals AST-H59 and AST-E1 to be $\sim$1.5–2.0‰ lower in $\delta^{18}O$ than azooxanthellate AST-AZ from the same site (Table 3). Although all three *Astrangia* show offsets from expected Δ_{47} that are smaller than those in *Porites*, there is no obvious difference in Δ_{47} between azooxanthellate and zooxanthellate specimens. This suggests that the presence of symbionts does not have a detectable effect on carbonate clumped isotope variability and is not the primary cause of the higher than expected Δ_{47} observed in *Porites*.

The presence of symbionts does not necessarily govern calcification rate however, and some azooxanthellate corals can achieve calcification rates comparable to zooxanthallate corals (Marshall, 1996). As such, calcification rate could be a mechanism for the positive Δ_{47} offsets we measure. Growth rates have been shown to be an important control on $\delta^{18}O$ in Red Sea *Porites*, with values closest to equilibrium in the slowest growing colonies and values furthest from equilibrium occurring at growth rates above $\sim$0.6 cm yr^{-1} (Felis et al., 2003). Similarly, the lowest intra-colony $\delta^{18}O$ values occur along a coral's maximum growth axis, and increase toward predicted equilibrium in regions of slower, lateral growth (McConnaughey, 1989a). To evaluate growth effects on coral Δ_{47} it would be ideal to know instantaneous calcification rates. However, to

our knowledge such data do not exist, and we estimated calcification rates for each of the corals in this study based on measurements at daily to annual timescales.

The annual mean calcification rate of RIB-B54 was calculated to be 3.90 ± 1.23 mg cm^{-2} d^{-1} using the product of linear extension and annual skeletal density (Lough and Barnes, 1997; Lough, 2008). We estimate the calcification rate of Red Sea *Porites* for which density data are not available from their linear extension rates using a relationship derived from 49 Indo-Pacific and Arabian Sea *Porites* (Lough, 2008):

$$\text{calcification } (\text{g cm}^{-2}\ \text{yr}^{-1}) = 0.105 \times \text{extension } (\text{mm yr}^{-1}) + 0.282; \quad r^2 = 0.93 \qquad (1)$$

Based on a mean extension rate of 11.9 ± 0.7 mm yr^{-1} (Felis et al., 2003), we estimate a mean EILAT-15B calcification rate of 4.20 ± 0.20 mg cm^{-2} d^{-1}. Similarly, using a BRI-1 extension rate of 15.8 ± 1.5 mm yr^{-1} that was estimated from the distance between the $\delta^{18}O$ maxima and minima presented in Ghosh et al. (2006), we calculate a calcification rate of 5.32 ± 0.43 mg cm^{-2} d^{-1}. The calcification rates of all other corals were calculated independently from Eq. (1). The mean extension and density of BAH-SID, measured by computed tomography, calculates a lower calcification rate of 1.12 ± 0.12 mg cm^{-2} d^{-1}. Furthermore, a calcification rate of 0.40 ± 0.05 mg cm^{-2} d^{-1} has been estimated for zooxanthallate *Astrangia* corals grown at 15 °C and various light intensities (Jacques et al., 1983). This value is statistically identical to the 0.36 ± 0.06 mg cm^{-2} d^{-1} estimated for *Astrangia* grown under the same conditions without symbionts (Jacques et al., 1983). Although poorly constrained, extension rates of 0.88–2.02 mm yr^{-1} have been estimated for deep sea *Caryophyllia* corals (Squires, 1960), and agree well with more robust estimates of 0.5–2.0 mm yr^{-1} in *Desmophyllum* corals (Cheng et al., 2000; Adkins et al., 2002; Adkins et al., 2004). Using these extension rates and a density of ~2.5 g cm^{-3} measured in southern ocean *Caryophyllia* (Thresher et al., 2011) we estimate a *Caryophyllia* calcification rate of 1.0 ± 0.4 mg cm^{-2} d^{-1}.

Comparing these estimates to the clumped isotope data suggests that deviations from expected Δ_{47} generally increase with faster calcification rates (Fig. 5). More slowly calcifying *Astrangia* and *Caryophyllia* corals are close to, or within the range of, values measured in inorganic experiments (Ghosh et al., 2006), while the largest Δ_{47} offsets occur in rapidly calcifying hermatypic corals. The range of Δ_{47} offsets evident in sub-annual *Porites* data is likely a consequence of our estimated calcification rates, which do not account for intra-annual growth variability. However, if we assume Δ_{47} offsets are positively correlated with calcification, the tendency toward smaller offsets during warm months (Fig. 4) implies that calcification rates may be reduced during summer. Assuming a constant seawater $\delta^{18}O$ value of 1.86‰ (Al-Rousan et al., 2003), sub-annual $\delta^{18}O$ offsets from the value predicted by Grossman and Ku (1986) are also smallest during warm months and are consistent with slower summer calcification rates in Red Sea *Porites* (Electronic Supplement Table 4). Although not intuitive, warm temperatures can suppress calcification rates in Red Sea corals (Cantin et al., 2010) due to declines in zooxanthellae photosynthetic capacity that reduce the availability of photosynthate that drives calcification (Jones et al., 1998; Al-Horani et al., 2003). We therefore hypothesize that a seasonal growth rate cycle, in which calcification is enhanced during winter and reduced in summer, may cause the small seasonal differences in Δ_{47} offset possibly observed in both BRI-1 and EILAT-15B (Fig. 4).

A link between calcification rate and Δ_{47} offset is supported by measurements along an isochron of variable growth rate in *Porites* coral 21-141-B11 (Fig. 1). Assuming the mean density measured in 21-141-B11 (1.59 ± 0.04 g cm^{-3}) is constant, the 0.23–0.81 cm yr^{-1} range in extension rate is equivalent to calcification rates of 1.0–3.5 mg cm^{-2} d^{-1}. Corresponding Δ_{47} data show a value of 0.687 ± 0.008‰ (1 s.e.) along the maximum growth axis that is offset from the Ghosh et al. (2006) calibration by 0.042 ± 0.008‰ similar to other *Porites* corals (Tables 3 and 4). Despite a constant temperature, Δ_{47} offsets generally decreases with growth rate – reaching an offset of 0.019‰ at the slowest calcification rate (Fig. 5). Consistent with the work of McConnaughey (1989a,b), this trend is accompanied by higher $\delta^{18}O$ and $\delta^{13}C$ at slower growth rates (Table 4). Although all 21-141-B11 Δ_{47} offsets are within the bounds of other *Porites* data, their tendency to decrease at slow growth rates is generally consistent with our hypothesized relationship with calcification rate. Similar macro-scale heterogeneities may explain the difference in bulk BRI-1 Δ_{47} values between Thiagarajan et al. (2011) and this study (Fig. 2b and c). Considering that these intra-coral differences cannot be explained by temperature, they are likely to reflect a kinetic or vital effect associated with calcification rate.

3.4. Calcification rate in other inorganic and biogenic marine carbonates

If calcification rate was responsible for higher than expected coral Δ_{47} values, we would expect the inorganic precipitation experiments upon which Δ_{47}-temperature calibrations are based to have significantly slower precipitation rates. The precipitation rates of the carbonates used in Δ_{47}-temperature calibration (Ghosh et al., 2006; Dennis and Schrag, 2010) were not formally calculated, but they can be estimated using the $\delta^{18}O$ values of those experiments. Using an experimental setup that differs from that of the Δ_{47}-temperature calibrations of Ghosh et al. (2006), Dietzel et al. (2009) suggest that calcite–water oxygen isotope fractionation varies with precipitation rate at 25 °C and pH = 8.3 following the relationship:

$$1000 \ln \alpha = -1.094 \log R + 30.87 \qquad (2)$$

where R is precipitation rate in μmol m^2 h^{-1}. Although the precipitation method used to generate Eq. (2) differs from that used by Ghosh et al. (2006) it may provide a valuable first-order estimate of precipitation rate. As discussed below, if the competition between precipitation rate and dissolved inorganic carbon DIC–H_2O isotope exchange is an important control on oxygen isotope fractionation, it is likely to affect both Ghosh-like and Dietzel-like methods.

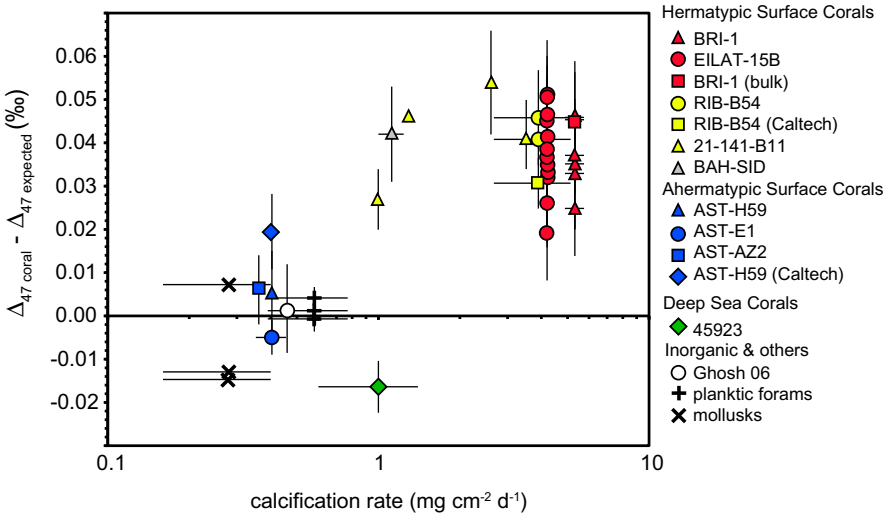

Fig. 5. Deviation of coral Δ_{47} from the expected value plotted versus calcification rate. Also shown are replicated planktic foraminifera (Tripati et al., 2010), mollusks (Came et al., 2007) and inorganic precipitation (Ghosh et al., 2006) data. Please see the online full color version.

Applying Eq. (2) to inorganic calcites precipitated at 25 °C by Kim and O'Neil (1997) and Dennis and Schrag (2010) suggests R values that are equivalent to precipitation rates of ~0.1 mg cm^{-2} d^{-1}. Ghosh et al. (2006) do not precipitate calcite at 25 °C, but their 1000 lnα–temperature relationship can be used to interpolate the fractionation factor expected at 25 °C. Using Eq. (2), the resulting 1000 lnα value estimates a slightly faster precipitation rate of 0.46 mg cm^{-2} d^{-1}. Although subject to significant uncertainty, these values suggest that the inorganic experiments used to calibrate the carbonate clumped isotope thermometer were likely precipitated at rates that are an order of magnitude slower than most hermatypic corals (Fig. 5).

In comparison to corals, other marine biogenic carbonates also calcify at slower rates that are significantly closer to those of inorganic precipitation experiments. For example, the calcification rate of the planktic foraminifera *Orbulina universa* has been estimated to be 0.58 ± 0.19 mg cm^{-2} d^{-1} (Lea et al., 1995) and mature *Arctica islandica* mollusks can have extension rates of <0.5 mm yr^{-1} (Kilada et al., 2007) that are equivalent to calcification rates of 0.16–0.4 mg cm^{-2} d^{-1} (using densities ranging from mean Great Barrier Reef *Porites*: 1.17 g cm^{-3}; Lough and Barnes, 1997, to pure aragonite: 2.93 g cm^{-3}). These slowly calcifying organisms generally have Δ_{47} values that are within error of those expected from inorganic calibrations and known growth temperatures (Came et al., 2007; Tripati et al., 2010; Fig. 5). The simplest explanation for these observations is that nearly all previously measured biogenic carbonates precipitate at rates near those of slow inorganic calibration experiments, while kinetic or vital effects associated with rapid calcification lead to deviations from expected Δ_{47} in hermatypic corals.

This possibility is supported by a recent inorganic precipitation experiment in which carbonate was rapidly precipitated at pH 9 and temperatures of 7, 25, 35 and 45 °C (Schmid, 2011). Although the Δ_{47} values of these samples should be interpreted cautiously given that they were measured using a new and unproven Kiel Device method (Schmid and Bernasconi, 2010), they show a temperature sensitivity similar to the Ghosh et al. (2006) inorganic calibration, but an intercept offset toward higher Δ_{47} (Fig. 3). Unfortunately, the precipitation rate of these experiments cannot be estimated using Eq. (2) because all DIC was consumed to form calcite (Schmid, 2011). In this case, calcite $\delta^{18}O$ must reflect the total number of ^{18}O and ^{16}O atoms in the solution, which is controlled by DIC speciation and should be independent of precipitation rate. However, Schmid (2011) reports fast precipitation and a relatively short experimental time that yields Δ_{47} values that are consistent with our coral data. This provides additional evidence that fast calcification may cause higher than expected Δ_{47} in surface corals.

3.5. Possible mechanisms for vital effects

3.5.1. Coral calcification

A discussion of mechanisms capable of causing Δ_{47} offsets in hermatypic corals is aided by a brief review of their calcification process. Although the specifics of this process are debated, it is generally agreed that corals calcify from a closed, or semi-enclosed, extracellular calcifying fluid that is isolated between existing coral skeleton and the coral's calicoblastic membrane (Fig. 6). Beginning from seawater, calcium concentrations in the calcifying space are elevated via a Ca-ATPase enzymatic pump that expels two protons for each Ca^{2+} pumped in (Ip et al., 1991; Cohen and McConnaughey, 2003). The removal of H^+ increases pH and shifts DIC speciation from HCO_3^- towards CO_3^{2-}, which in turn increases the aragonite saturation state (Ω) of the calcifying fluid (Cohen and McConnaughey, 2003). Attempts to quantify this process through live tissue imaging (Venn et al., 2011), micro-electrode measurements (Al-Horani et al., 2003), boron isotopes (Rollion-Bard

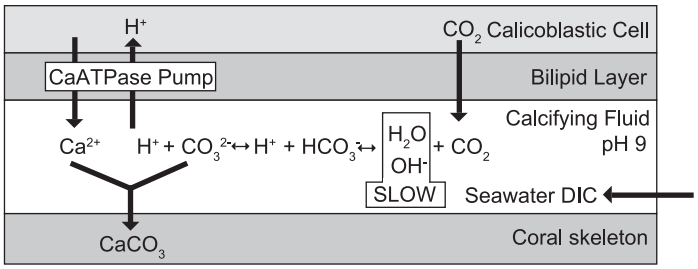

Fig. 6. Simplified schematic diagram of coral calcification. See the text for a detailed explanation. Not to scale.

et al., 2003; Rollion-Bard et al., 2011) and comparison of coral and abiogenic aragonite (Holcomb et al., 2009) suggest that a calcifying fluid pH of ~9.0 can elevate supersaturation to $\Omega \approx 25$. The pumping of protons out of the calcifying space also reduces the partial pressure of CO_2 within the calcifying fluid, leading to a diffusive flux of respired CO_2 through the calicoblastic membrane into the calcifying space. This metabolic CO_2 can then react to form HCO_3^- and CO_3^{2-} through hydration and/or hydroxylation depending on pH:

$$\text{Hydration}: CO_2 + H_2O \leftrightarrows H_2CO_3 \leftrightarrows H^+ + HCO_3^- \leftrightarrows H^+ + CO_3^{2-} \quad (3)$$

$$\text{Hydroxylation}: CO_2 + OH^- \leftrightarrows HCO_3^- \leftrightarrows H^+ + CO_3^{2-} \quad (4)$$

Because the calcifying space is not a perfectly closed system, additional seawater DIC may also leak into the calcifying space, providing an additional carbon source for calcification (Fig. 6).

3.5.2. Previous models of carbon and oxygen isotope vital effects in corals

The basic model for coral biomineralization discussed above has been used as the basis for a number of explanations for $\delta^{18}O$ and $\delta^{13}C$ vital effects that may also be relevant to Δ_{47}. For example, McConnaughey (1989a,b) proposed a kinetic model to explain trends in coral $\delta^{18}O$ and $\delta^{13}C$ offsets. This model argues that because DIC oxygen isotopes equilibrate slowly with water at high pH (Mills and Urey, 1940), metabolic CO_2 entering the coral calcifying space may not reach oxygen isotopic equilibrium with the calcifying fluid prior to skeletal formation. The forward and backward reactions of Eqs. (3) and (4) must occur 15 times for oxygen isotopes to reach 99% equilibration and the equilibration time of this system is about 44 h (Zeebe and Wolf-Gladrow, 2001). If the isotopic equilibration through hydration/dehydration and hydroxylation/dehydroxylation reactions (Eqs. (3) and (4)) is outpaced by rapid coral calcification, calcifying fluid DIC would not reach isotopic equilibrium and the coral skeleton would inherit the disequilibrium signal of the calcifying fluid. Because of discrimination against ^{18}O during hydration and hydroxylation, it was argued that this isotopic disequilibrium should lead to ^{18}O-depleted HCO_3^- and lower skeletal $\delta^{18}O$ when coral growth was rapid (McConnaughey, 1989a,b). Proportional decreases in $\delta^{13}C$ were explained by kinetic carbon isotope fractionations of −13‰ and −27‰ for hydration and hydroxylation, respectively (Siegenthaler and Münnich, 1981; O'Leary et al., 1992).

Adkins et al. (2003) also observed proportional $\delta^{18}O$ and $\delta^{13}C$ decreases in azooxanthellate deep-sea corals, but explained them using an equilibrium model rather than a kinetic one. Because the oxygen isotope fractionation factor between HCO_3^- and water is larger than that between CO_3^{2-} and water, $\delta^{18}O$ of total precipitated carbonate decreases as the CO_3^{2-} becomes a larger fraction of DIC (McCrea, 1950; Usdowski et al., 1991; Spero et al., 1997; Zeebe, 1999; Beck et al., 2005; Kim et al., 2006; Dietzel et al., 2009). Adkins et al. (2003) therefore suggested that low $\delta^{18}O$ in dense skeletal regions reflects faster calcification from a high pH calcifying fluid in which CO_3^{2-} is the dominant DIC species. An increasing $\delta^{18}O$ trend in less dense aragonite could then be explained by progressively lower calcifying fluid pH and decreasing CO_3^{2-} concentrations. Deviations of $\delta^{13}C$ from equilibrium were explained separately using the relative proportion of DIC derived from seawater and from aqueous CO_2 that diffuses across the cell membrane into the calcifying space. Specifically, at low pH and slow calcification rates, seawater DIC mixes thoroughly with the calcifying fluid leading to relatively high $\delta^{13}C$ that is near equilibrium. In contrast, the diffusive flux of isotopically light aqueous CO_2 into the calcifying space increases at high pH and faster calcification rates, leading to low $\delta^{13}C$ that is furthest from equilibrium.

Rollion-Bard et al. (2003) proposed a hybrid of the two models to explain fine scale variations in $\delta^{18}O$, $\delta^{13}C$ and boron isotopes in a *Porites* coral. In this model, $\delta^{18}O$ vital effects are attributed to variations in the pH of the calcifying fluid and the residence time of DIC in that fluid prior to calcification. Although high calcifying fluid pH would favor lower coral $\delta^{18}O$ by shifting DIC speciation toward CO_3^{2-}, it would also lead to slower equilibration between DIC and water that could induce additional hydration/hydroxylation kinetic effects, especially when DIC residence time is short. Using this approach, Rollion-Bard et al. (2003) could explain the majority of the $\delta^{18}O$ vital effects they observed using a DIC residence time of 1–12 h. The fast equilibration of carbon isotopes lead to little fine scale variations and Rollion-Bard et al. (2003) suggested coral $\delta^{13}C$ was primarily controlled by the relative amounts of metabolic CO_2 and seawater DIC incorporated into the skeleton.

These models share a number of variables including (1) the pH of the calcifying fluid (2) the relative rates of DIC

equilibration and skeleton precipitation and (3) the proportion of DIC derived from metabolic CO_2 versus the amount derived from seawater. Evaluating these processes in terms of Δ_{47} may help elucidate the cause for positive Δ_{47} offsets in rapidly calcifying corals and help identify different calcification mechanisms among different species.

3.5.3. pH

As discussed by Thiagarajan et al. (2011), differences in clumped isotope composition between DIC species could lead to pH effects in Δ_{47}. Based on theoretical calculations, CO_3^{2-} is estimated to be ~0.018‰ lower in Δ_{47} than HCO_3^- (Guo, 2008; Thiagarajan et al., 2011). The equivalent $\delta^{18}O$ difference between CO_3^{2-} and HCO_3^- varies subtly between studies, but suggests CO_3^{2-} is ~7.0‰ lower at 25 °C (Beck et al., 2005; Kim et al., 2006).

Assuming the experiments of Ghosh et al. (2006) were conducted at near neutral pH where HCO_3^- is the dominant DIC species, departures from apparent equilibrium due to increased pH should result in lower $\delta^{18}O$ and Δ_{47} values. DIC is ~90% HCO_3^- and ~10% CO_3^{2-} at pH 8 and ~47% HCO_3^- and ~53% CO_3^{2-} at pH 9, which is typical for coral calcifying fluid (Based on the CO2SYS program, Pierrot et al., 2006; S = 35 psu, $T = 25$ °C, $TCO_2 = 2100$ μmol/kgSW, seawater pH scale). A carbonate ion increase of this magnitude is expected to lower $\delta^{18}O$ by ~3.7‰ and Δ_{47} by ~0.01‰. Consistent with the models of Adkins et al. (2003) and Rollion-Bard et al. (2003), this mechanism can explain the direction and magnitude of coral $\delta^{18}O$ offsets. However, the predicted pH effect cannot explain the positive Δ_{47} offsets observed in shallow water, hermatypic corals (Fig. 7). In contrast, ahermatypic coral data shows negative $\delta^{18}O$ offsets that are not accompanied by significant Δ_{47} offsets, consistent with a pH mechanism and the results of Thiagarajan et al. (2011) (Fig. 7). Although the influence of DIC speciation on Δ_{47} warrants further investigation, current understanding does not support a pH influence of either the correct sign or magnitude to explain the hermatypic coral Δ_{47} data.

3.5.4. Hydration and hydroxylation

Experiments indicate that the CO_2–H_2O oxygen isotope exchange rate for Δ_{47} is similar to that for $\delta^{18}O$ (Affek et al., 2009). This suggests that any $\delta^{18}O$ kinetic effects associated with incomplete DIC–H_2O equilibration through hydration/dehydration and hydroxylation/dehydroxylation (Eqs. (3) and (4)) should be accompanied by proportional Δ_{47} offsets. Coordinated $\delta^{18}O$ and Δ_{47} offsets are supported by preliminary theoretical calculations of the kinetic effects associated with the net forward hydration/hydroxylation reactions, which suggest that Δ_{47} would increase by 0.01–0.05‰ for every 1‰ decrease in $\delta^{18}O$ (Guo et al., 2009). Because this is a relatively large range of Δ_{47} variability, additional insight into the proportional offsets associated with hydration/hydroxylation may be provided by comparisons with dehydration/dehyroxylation kinetic fractionations during CO_2 degassing in the context of speleothem precipitation (Guo, 2008). Like corals, speleothems precipitate rapidly from a supersaturated solution. However, unlike corals where CO_2 is thought to diffuse into the calcifying space, speleothem precipitation occurs when CO_2 is removed from supersaturated drip water. Degassing of CO_2 during speleothem formation can occur through either bicarbonate dehydration or dehydroxylation reactions, which are essentially the reverse of Eqs. (3) and (4)

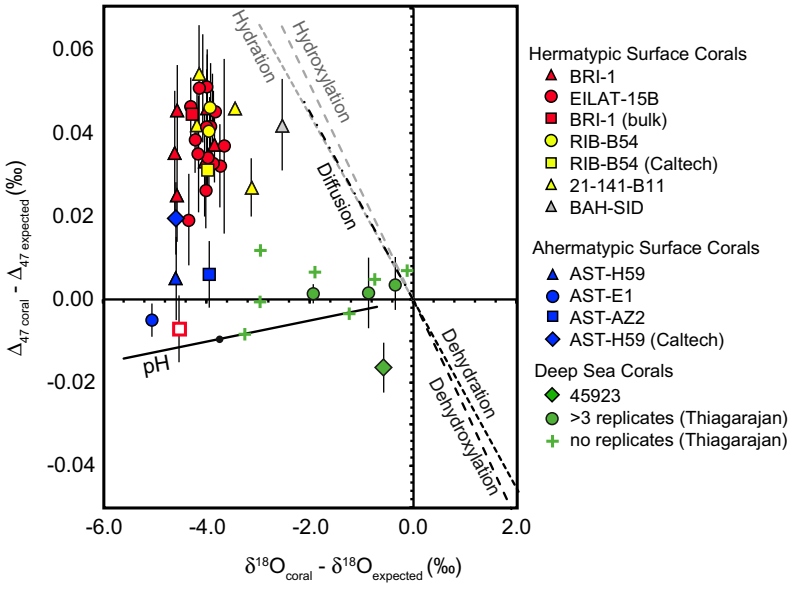

Fig. 7. Deviation of measured coral Δ_{47} and $\delta^{18}O$ from that expected based on the calibrations of Ghosh et al. (2006) and Grossman and Ku, 1986. Also shown are the deviations expected for elevated calcifying fluid pH, CO_2 diffusion into the calcifying space and hydration/hydroxylation of CO_2 within the calcifying space (estimated as the extension of dehydration/dehyroxylation). The offsets expected at pH 9 (dot) is marked on the pH vector. See Electronic Supplement Table 4 for seawater $\delta^{18}O$ values used to calculate $\delta^{18}O$ offsets. Please see the online full color version.

described above. Calculations of the dehydration kinetic effect predict that at 25 °C, a 1‰ enrichment in $\delta^{18}O$ would be accompanied by a 0.022‰ decrease in Δ_{47} and a 3.26‰ increase in $\delta^{13}C$ (Guo, 2008; Figs. 7 and 8). Similar calculations for dehydroxylation predict a Δ_{47} decrease of 0.026‰ and a $\delta^{13}C$ increase of 1.41‰ (Figs. 7 and 8). Consistent with these values, speleothem data show higher than predicted $\delta^{18}O$, but lower than predicted Δ_{47} (Affek et al., 2008; Daëron et al., 2011; Kluge and Affek, 2012).

The $\delta^{18}O$, $\delta^{13}C$ and Δ_{47} offsets estimated from the inverse of Guo's (2008) dehydration/dehydroxylation calculations generally agree in sign and magnitude with preliminary hydration/hydroxylation calculations (Guo et al., 2009). We therefore consider these values to be a first order approximation of the Δ_{47} offsets associated with hydration/hydroxylation kinetic effects, and we expect these effects to cause lower than predicted $\delta^{18}O$ and $\delta^{13}C$, but higher than predicted Δ_{47} in carbonates. This is generally consistent with the sign of $\delta^{18}O$, $\delta^{13}C$ and Δ_{47} offsets observed in our coral data (Figs. 7 and 8), suggesting that hydration/hydroxylation kinetics may be a primary source of positive Δ_{47} offsets. As discussed below, deviations from the hydration/hydroxylation vectors in Figs. 7 and 8 may stem from uncertainties in theoretical calculations and/or from additional processes that contribute to a combined vital effect.

Hydration/hydroxylation kinetics would only influence metabolic CO_2, not ambient seawater DIC, which would already be equilibrated upon entering the calcifying space. Therefore, any influence of hydration/hydroxylation on coral Δ_{47} would depend on the ratio of metabolic CO_2 to seawater DIC in the calcifying space. Estimates of this ratio vary, but studies of symbiotic corals suggest the majority (~75%) of skeleton derives from metabolic CO_2 (Erez 1978; Furla et al., 2000a), while asymbiotic deep-sea coral skeleton is constructed in large part (>90%) from ambient DIC (Griffin and Druffel, 1989; Adkins et al., 2003).

Based on these observations, we hypothesize that Δ_{47} offsets are observed in fast growing hermatypic corals in part because they form their skeletons primarily from metabolic CO_2. A heavy reliance on metabolic CO_2 may increase the kinetic effects associated with hydration/hydroxylation when the rate of calcification is faster than DIC equilibration, leading to positive Δ_{47} offsets and negative $\delta^{18}O$ offsets (Fig. 7). Furthermore, $\delta^{18}O$ and $\delta^{13}C$ offsets always lie within the range predicted by Guo (2008) for hydration/hydroxylation kinetic effects, providing additional support for this mechanism (Fig. 8). A hydration/hydroxylation kinetic effect is also consistent with the tendency for $\delta^{18}O$, $\delta^{13}C$ and Δ_{47} offsets to approach their expected values in slower growing portions of the *Porites* 21-141-B11 isochron (Figs. 7 and 8). We suggest this trend may reflect longer DIC residence times in slower growing portions of the skeleton, which permit greater equilibration of metabolic CO_2 with water prior to precipitation.

Similarly, deep-sea corals show little or no Δ_{47} offset for two reasons. First, their skeletons are derived primarily from ambient seawater DIC that does not require hydration/hydroxylation within the calcifying fluid. Second, their slow growth implies longer calcifying fluid residence times that may allow for DIC equilibration. Consistent with this hypothesis, relatively slowly calcifying foraminifera also incorporate little metabolic CO_2 into their skeletons (Spero and Lea, 1996) and generally agree with inorganic Δ_{47} calibrations (Tripati et al., 2010). Although deep-sea corals exhibit $\delta^{18}O$ and $\delta^{13}C$ offsets that are consistent with hydration/hydroxylation effects (Fig. 8), their small Δ_{47}

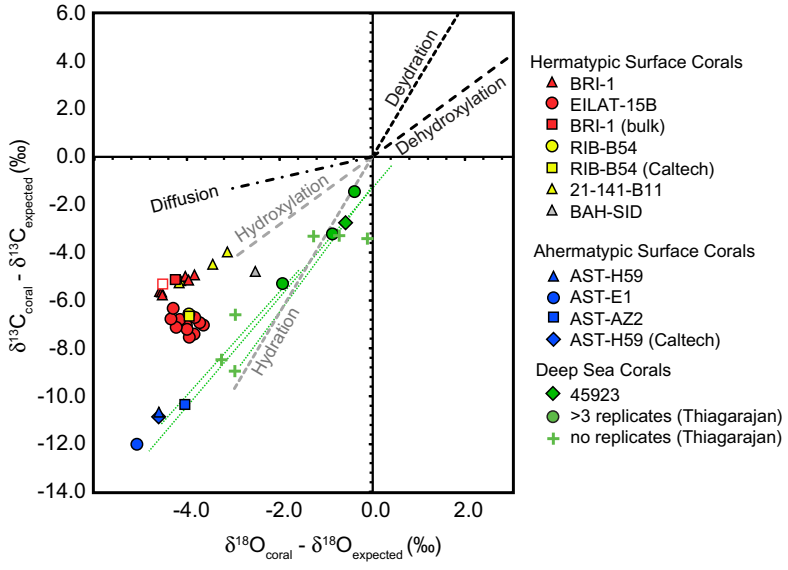

Fig. 8. Deviation of measured coral $\delta^{13}C$ and $\delta^{18}O$ from that expected from the data of Romanek et al. (1992) and Grossman and Ku (1986). Also shown are the deviations expected for CO_2 diffusion into the calcifying space and hydration/hydroxylation of CO_2 within the calcifying space (estimated as the extension of dehydration/dehyroxylation effects calculated by Guo (2008)). Corals with little or no Δ_{47} offset show $\delta^{13}C$ and $\delta^{18}O$ offset trends that are similar to previously measured deep-sea corals (dotted lines; Adkins et al., 2003) suggesting that this vector may be a hallmark of isotopically equilibrated calcifying fluid. See Electronic Supplement Table 4 for the seawater DIC $\delta^{13}C$ values used to calculate $\delta^{13}C$ offsets. Please see the online full color version.

offset suggests a near equilibrium DIC pool that does not agree with this kinetic mechanism. Instead, deep-sea coral data may be better explained by an equilibrium model in which increases in the pH of calcifying fluid cause lower coral $\delta^{18}O$ (Adkins et al., 2003), without changing Δ_{47} appreciably (see Section 3.5.3). Although Adkins et al. (2003) predict pH increases up to ~10.5 that are higher than observed (Al-Horani et al., 2003; Venn et al., 2011), their model suggests that elevated pH will increase the flux of low $\delta^{13}C$ aqueous CO_2 into the calcifying space, leading to negative $\delta^{13}C$ offsets. It is critical to note that, unlike the hydration/hydroxylation kinetic mechanism, the CO_2 in the Adkins et al. (2003) model undergoes full oxygen isotope exchange with water, and explains why $\delta^{13}C$ offsets are not accompanied by large Δ_{47} offsets in deep-sea corals (Thiagarajan et al., 2011).

Because the ratio of metabolic to seawater DIC incorporated into coral skeleton appears to depend loosely on the presence of symbionts, it is somewhat surprising that zooxanthellate and azooxanthellate *Astrangia* corals both show little or no Δ_{47} offset. We suggest that this may be caused by the slow calcification rate of *Astrangia*, which could be sufficiently sluggish to allow full DIC equilibration even when the majority of skeleton is formed from metabolic CO_2. If this is the case, large $\delta^{18}O$ and $\delta^{13}C$ offsets could still be explained using the model of Adkins et al. (2003).

The argument for a hydration/hydroxylation kinetic effect relies on DIC within the calcifying space not reaching equilibrium. Carbonic anhydrase (CA) is a metalloenzyme that catalyzes the hydration of CO_2 and significantly reduces the time needed to reach isotopic equilibrium (Silverman, 1982). Using abiogenic carbonates precipitated at varying CA concentrations, Uchikawa and Zeebe (2012) constructed a model that clearly shows the time necessary to reach oxygen isotopic equilibrium decreases significantly with increasing concentrations of the enzyme. At the highest CA concentrations studied (1.8×10^{-8} mol/L), equilibrium was reached in ~20 min at pH 8 compared with ~5 h in experiments without the catalyst. At pH 9, equilibrium was achieved in ~3 h in the presences of CA, while over 16 h was required in its absence (Uchikawa and Zeebe, 2012).

Experiments that inhibit carbonic anhydrase in corals typically show reduced calcification rates (Furla et al., 2000b; Al-Horani et al., 2003) and the enzyme has been located in the calicoblastic ectoderm (Moya et al., 2008), suggesting that it is present and active within the calcifying space. Assuming the equilibration time predicted by Uchikawa and Zeebe (2012) at pH 9 is appropriate for the calcifying fluid, a kinetic hydration/hydroxylation effect would be unlikely if the residence time of DIC in the calcifying fluid is longer than ~3 h. The residence time of calcifying fluid is poorly known, but has been estimated to be between 30 min and 12 h (McConnaughey, 1989b; Furla et al., 2000a; McConnaughey, 2003; Rollion-Bard et al., 2003; Gagnon et al., 2012). Assuming the residence time of DIC does not exceed that of the calcifying fluid, this raises the possibility that hydration/hydroxylation kinetic effects could occur even in the presence of CA. Indeed, at least some of the scatter among $\delta^{18}O$, $\delta^{13}C$ and Δ_{47} offsets in hermatypic corals could be caused by different CA activity and/or calcifying fluid residence times. Although future work is necessary to improve estimates of the residence time and CA concentration of the calcifying fluid, kinetic fractionation during hydration/hydroxylation is a likely source for positive Δ_{47} offsets in shallow water corals.

3.5.5. Diffusion

Thiagarajan et al. (2011) suggested that diffusion of CO_2 across the calicoblastic membrane into the calcifying fluid could cause kinetic fractionations of Δ_{47}. Diffusion may also contribute to kinetic effects if a diffusive boundary layer develops between the growing mineral surface and the bulk calcifying fluid when coral growth is fast. In either case, Thiagarajan et al. (2011) argue that liquid phase diffusion of CO_2 would lead to 0.7‰ and 1.6‰ decreases in $\delta^{13}C$ and $\delta^{18}O$, respectively, and a 0.036‰ increase in Δ_{47}. These $\delta^{18}O$ and Δ_{47} offsets are generally consistent with our coral data (Fig. 7), but the complementary $\delta^{13}C$ offset underestimates the values typically observed in corals (Fig. 8). Although it is premature to rule out diffusion as a mechanism for vital effects in coral Δ_{47}, its underestimation of observed $\delta^{13}C$ offsets suggest it is not the primary cause.

Furthermore, like a hydration/hydroxylation kinetic effect, an effect associated with CO_2 diffusion across the calicoblastic membrane into the calcifying fluid would not impact seawater DIC leaking into the calcifying space. Thus, its influence would depend on the relative contributions of metabolic CO_2 and ambient seawater DIC to coral skeleton. In a strict sense, CO_2 diffusion across the calicoblastic membrane would not be influenced directly by the presence or absence of CA since CA does not affect the rate of diffusion. However, the degree to which the coral skeleton inherits a kinetic effect associated with CO_2 diffusion across the calicoblastic membrane will be impacted by CA activity through its influence on CO_2–H_2O isotope exchange. For example, if CA allows isotopic equilibrium to be achieved, any kinetic effect associated with CO_2 diffusion across the calicoblastic membrane will be erased. In contrast, if CA is either not active, or does not achieve complete isotopic equilibration through hydration/hydroxylation of CO_2 following its diffusion into the calcifying space, kinetic effects related to CO_2 diffusion across the calicoblastic membrane may contribute to Δ_{47} offsets in surface corals.

3.5.6. Combined effects

It is likely that no mechanism is solely responsible for the positive Δ_{47} offsets we observe in corals. Indeed, when taken at face value, none of the mechanisms hypothesized to produce coordinated Δ_{47}, $\delta^{18}O$ and $\delta^{13}C$ offsets in Figs. 7 and 8 perfectly describe our coral data. Although analytical and theoretical uncertainties likely contribute to these discrepancies, they also may reflect the combination of multiple effects. For example, simple vector addition suggests that the combined effect of hydration/hydroxylation (which underestimates $\delta^{18}O$ offsets relative to the Δ_{47} offsets observed) and pH (which leads to negative $\delta^{18}O$ offsets without changing Δ_{47} appreciably) may explain hermatypic coral offsets better than any single mechanism. Therefore, a multivariate approach may better describe Δ_{47} variability,

and we suggest future work should focus not only on isolating the signature of individual mechanisms (i.e. diffusion, pH, hydration/hydroxylation, etc.), but also their cumulative effects. Furthermore, sufficient data is not yet available to evaluate a number of mechanisms that may contribute to Δ_{47} vital effects in hermatypic corals including attachment–detachment kinetics at the mineral–fluid boundary, transport limitations in the fluid, solid state diffusion and Rayleigh fractionation (Watson, 2004; Gaetani and Cohen, 2006; DePaolo, 2011). Assessing the impact of these mechanisms and incorporating their effects into a multivariate approach will likely further improve our understanding of the processes driving Δ_{47} variability in shallow water corals.

3.5.7. The utility of carbonate clumped isotope thermometry in shallow water corals

Although the presence of vital effects complicates the interpretation of carbonate clumped isotope variability in shallow water corals, Δ_{47} shows a clear temperature dependence and may still be a valuable paleotemperature proxy. Realizing the full potential of the Δ_{47} proxy will require avoiding and/or correcting for these vital effects. Evidence that Δ_{47} vital effects are correlated with calcification rate suggests that they may be minimized or avoided by sampling slower growing portions of shallow water corals. Evaluating this possibility will require future work that investigates intra-coral Δ_{47} variability across a wider range of growth rates and coral species. Furthermore, corals with little or no Δ_{47} offset typically show a common linear trend in $\delta^{18}O$ and $\delta^{13}C$ offsets, while corals with significant Δ_{47} offsets deviate from this trend and show smaller $\delta^{13}C$ offsets for a given $\delta^{18}O$ offset (Fig. 8). As discussed in Section 3.5.4, the linear trend in $\delta^{18}O$ and $\delta^{13}C$ offsets among corals with little or no Δ_{47} offset can be explained by equilibrium processes (Adkins et al., 2003), and may be a hallmark of equilibrated calcifying fluid. If this is the case, this line may be used to screen for coral samples likely to have large Δ_{47} offsets prior to conducting time consuming clumped isotope analyses.

Correcting for Δ_{47} vital effects may also be possible. If future work identifies a relatively constant Δ_{47} offset in all shallow water corals, this value may simply be subtracted to yield more accurate temperature estimates. The identification of a constant offset seems unlikely however, and a reliable means of correcting for vital effects will likely require an improved understanding of the mechanisms responsible for Δ_{47} offsets in corals. Experiments that precipitate aragonite rapidly at elevated pH and known temperatures will be particularly valuable. For example, better quantifying the influence of temperature and precipitation rate on Δ_{47} and other paleoproxies may allow for accurate paleotemperature estimates through a multi-proxy approach.

4. SUMMARY AND CONCLUSIONS

We present the first survey of carbonate clumped isotope variability in shallow water corals. Hermatypic corals consistently show higher than expected Δ_{47} that underestimates temperature by ~8 °C, while ahermatypic corals generally agree with inorganic calibrations. Our data suggest that this deviation from expected Δ_{47} in hermatypic corals is unlikely to be explained by laboratory artifacts such as: (1) alteration via micromilling, (2) organic matter contamination, (3) interlaboratory differences in sample preparation or analysis. Furthermore, we measure similar Δ_{47} values in corals that grew at high and normal marine salinities, suggesting that salinity does not affect Δ_{47}. Similarly, we find no consistent difference in Δ_{47} values between corals with and without symbionts, indicating that the presence and/or absence of zooxanthallae does not impact Δ_{47}. Instead, we suggest that the rapid calcification of hermatypic corals may cause the Δ_{47} offsets. Current data suggests that pH-related changes in DIC speciation alone cannot explain the observed $\delta^{18}O$ and Δ_{47} offsets. The offsets predicted for diffusion of CO_2 into a coral's calcifying fluid are consistent with our Δ_{47} and $\delta^{18}O$ data, but do not accurately characterize the $\delta^{13}C$ offsets we observe. In contrast, a kinetic effect associated with hydration/hydroxylation successfully describes both the direction and magnitude of Δ_{47}, $\delta^{18}O$ and $\delta^{13}C$ offsets and is our preferred mechanism for shallow water coral vital effects. This kinetic effect is expressed in hermatypic corals because their skeletons derive largely from metabolic CO_2 and because their rapid precipitation may prevent complete DIC equilibration even when carbonic anhydrase is present. Subtle or no vital effects are observed in ahermatypic corals because their skeletons are constructed in large part from ambient seawater DIC and their slow growth rate favors complete equilibration of DIC with the calcifying fluid. Although these vital effects will complicate the interpretation of carbonate clumped isotope variability in shallow water corals in terms of SST, Δ_{47} shows a clear temperature dependence and may still be a valuable paleotemperature proxy.

ACKNOWLEDGMENTS

We thank Gerry Olack, Dominic Colosi and Glendon Hunsinger of the Yale Earth System Center for Stable Isotopic Studies for their laboratory assistance. Also thanks to members of the Affek lab for discussion and access to their data. Daniel Schrag, Jess Adkins and Robert Halley generously donated coral samples. Eric Matson and Eric Lazo-Wasem provided valuable logistical support. This work was supported by the NOAA Climate and Global Change Postdoctoral Program for C.S. and National Science Foundation Grant NSF-EAR-0842482 to H.P.A. T.F. is supported by the DFG-Research Center/Excellence Cluster "The Ocean in the Earth System".

APPENDIX A. SUPPLEMENTARY DATA

Supplementary data associated with this article can be found, in the online version, at http://dx.doi.org/10.1016/j.gca.2012.09.035.

REFERENCES

Adkins J. F., Griffin S., Kashgarian M., Cheng H., Druffel E. R. M., Boyle E. A., Edwards R. L. and Shen C.-C. (2002) Radiocarbon dating of deep-sea corals. *Radiocarbon* **44**, 567–580.

Adkins J. F., Boyle E. A., Curry W. B. and Lutringer A. (2003) Stable isotopes in deep-sea corals and a new mechanism for "vital effects". *Geochim. Cosmochim. Acta* **67**, 1129–1143.

Adkins J. F., Henderson G. M., Wang S.-L., O-Shea S. and Mokadem F. (2004) Growth rates of the deep-sea scleractinia *Desmophyllum cristagalli* and *Enallopsammia rostrata*. *Earth Planet. Sci. Lett.* **227**, 481–490.

Affek H. P., Bar-Matthews M., Ayalon A., Mathews M. and Eiler J. M. (2008) Glacial/interglacial temperature variations in Sorequ cave speleothems as recorded by 'clumped isotope' thermometry. *Geochim. Cosmochim. Acta* **72**, 5351–5360.

Affek H. P., Ayalon A., Bar-Matthews M. and Matthews A. (2009) Kinetic effects in 'clumped isotopes': application to Soreq cave speleothems. *Eos Trans. AGU* ***90,*** Fall Meet. Suppl. PP11F-07 (abstr.).

Ahmad F. and Sultan S. A. R. (1989) Surface heat fluxes and their comparison with the oceanic heat flow in the Red Sea. *Oceanol. Acta* **12**, 33–36.

Al-Horani F. A., Al-Moghrabi S. M. and de Beer D. (2003) The mechanism of calcification and its relation to photosynthesis and respiration in the scleractinian coral *Galaxea fascicularis*. *Mar. Biol.* **142**, 419–426.

Al-Rousan S., Al-Moghrabi S., Patzold J. and Wefer G. (2003) Stable oxygen isotopes in Porites corals monitor weekly temperature variations in the northern Gulf of Aquaba, Red Sea. *Coral Reefs* **22**, 346–356.

Barnes D. J. and Chalker B. E. (1990) Calcification and photosynthesis in reef-building corals and algae. In *Coral Reefs* (ed. Z. Dubinsky). Ecosystems of the World Elsevier, Amsterdam.

Beck W. C., Grossman E. L. and Morse J. W. (2005) Experimental studies of oxygen isotope fractionation in the carbonic acid system at 15° 25° and 40°C. *Geochim. Cosmochim. Acta* **69**, 3493–3503.

Came R. E., Eiler J. M., Veizer J., Azmy K., Brand U. and Weidman C. R. (2007) Coupling of surface temperatures and atmospheric CO_2 concentrations during the Palaeozoic era. *Nature* **449**, 198–201.

Cantin N. E., Cohen A. L., Karnauskas K. B., Tarrant A. M. and McCorkle D. C. (2010) Ocean warming slows coral growth in the central Red Sea. *Science* **329**, 322–325.

Carton J. A. and Giese B. S. (2008) A reanalysis of ocean climate using simple ocean data assimilation (SODA). *Mon. Weather Rev.* **136**, 2999–3017.

Cheng H., Adkins J. F., Edwards R. L. and Boyle E. A. (2000) U-Th dating of deep-sea corals. *Geochim. Cosmochim. Acta* **64**, 2401–2416.

Cohen A. L. and Hart S. R. (1997) The effect of colony topography on climate signals in coral skeleton. *Geochim. Cosmochim. Acta* **61**, 3905–3912.

Cohen A. L. and McConnaughey T. A. (2003) Geochemical perspectives on coral mineralization. In *Reviews in Mineralogy and Geochemistry: Biomineralization* (eds. Patricia M. Dove, Stev Weiner and James J. De Yoreo). Mineralogical Society of America, Washington, DC.

Cole J. E., Fairbanks R. G. and Shen G. T. (1993) Recent variability in the southern oscillation: isotopic results from a Tarawa Atoll coral. *Science* **260**, 1790–1793.

Daëron M., Guo W., Eiler J., Genty D., Blamart D., Boch R., Drysdale R., Maire R., Wainer K. and Zanchetta G. (2011) $^{13}C^{18}O$ clumping in speleothems: observations from natural caves and precipitation experiments. *Geochim. Cosmochim. Acta* **75**, 3303–3317.

DePaolo D. J. (2011) Surface kinetic model for isotopic and trace element fractionation during precipitation of calcite from aqueous solutions. *Geochim. Cosmochim. Acta* **75**, 1039–1056.

Dennis K. J. and Schrag D. P. (2010) Clumped isotope thermometry of carbonatites as an indicator of diagenetic alteration. *Geochim. Cosmochim. Acta* **74**, 4110–4122.

Dennis K. J., Affek H. P., Passey B. H., Schrag D. P. and Eiler J. M. (2011) Defining an absolute reference frame for 'clumped' isotope studies of CO_2. *Geochim. Cosmochim. Acta* **75**, 7117–7131.

Dietzel M., Tang J., Leis A. and Köhler S. J. (2009) Oxygen isotopic fractionation during inorganic calcite precipitation – effects of temperature, precipitation rate and pH. *Chem. Geol.* **268**, 107–115.

Dimond J. and Carrington E. (2007) Temporal variation in the symbiosis and growth of the temperate scleractinian coral *Astrangia poculata*. *Mar. Ecol. Prog. Ser.* **348**, 161–172.

Eiler J. M. (2011) Paleoclimate reconstruction using carbonate clumped isotope thermometry. *Quatern. Sci. Rev.* **30**, 3575–3588.

Eiler J. M. and Schauble E. (2004) $^{18}O^{13}C^{16}O$ in Earth's atmosphere. *Geochim. Cosmochim. Acta* **68**, 4767–4777.

Emiliani C. (1955) Pleistocene temperatures. *J. Geol.* **63**, 538–578.

Epstein S., Buchsbaum R., Lowenstam H. A. and Urey H. C. (1953) Revised carbonate-water isotopic temperature scale. *Geol. Soc. Am. Bull.* **64**, 1315–1326.

Erez J. (1978) Vital effect on stable-isotope composition seen in foraminifera and coral skeletons. *Nature* **273**, 199–202.

Felis T., Pätzold J., Loya Y., Fine M., Nawar A. H. and Wefer G. (2000) A coral oxygen isotope record from the northern Red Sea documenting NAO, ENSO, and North Pacific teleconnections on Middle East climate variability since the year 1750. *Paleoceanography* **15**, 679–694.

Felis T., Pätzold J. and Loya Y. (2003) Mean oxygen-isotope signatures in *Porites* spp. corals: inter-colony variability and correction for extension-rate effects. *Coral Reefs* **22**, 328–336.

Felis T., Lohmann G., Kuhnert H., Lorenz S. J., Scholz D., Pätzold J., Al-Rousan S. A. and Al-Moghrabi S. M. (2004) Increased seasonality in Middle East temperatures during the last interglacial period. *Nature* **429**, 164–168.

Furla P., Galgani I., Durand I. and Allemand D. (2000a) Sources and mechanisms of inorganic carbon transport for coral calcification and photosynthesis. *J. Exp. Biol.* **203**, 3445–3457.

Furla P., Allemand D. and Orsenigo M. N. (2000b) Involvement of H^+-ATPase and carbonic anhydrase in inorganic carbon uptake for endosymbiont photosynthesis. *Am. J. Physiol. – Regul. Integr. Comp. Physiol.* **278**, 870–881.

Gaetani G. A. and Cohen A. L. (2006) Element partitioning during precipitation of aragonite from seawater: a framework for understanding paleoproxies. *Geochim. Cosmochim. Acta* **70**, 4617–4634.

Gagnon A. C., Adkins J. F. and Erez J. (2012) Seawater transport during coral biomineralization. *Earth Planet. Sci. Lett.* **329–330**, 150–161.

Genin A., Lazar B. and Brenner S. (1995) Vertical mixing and coral death in the Red Sea following the eruption of Mount Pinatubo. *Nature* **377**, 507–510.

Ghosh P., Adkins J. F., Affek H., Balta B., Guo W., Schauble E. A., Schrag D. P. and Eiler J. M. (2006) $_{13}C–^{18}O$ bonds in carbonate minerals: a new kind of paleothermometer. *Geochim. Cosmochim. Acta* **70**, 1439–1456.

Ghosh P., Eiler J., Campana S. E. and Feeny R. F. (2007) Calibration of the carbonate 'clumped isotope' paleothermometer for otoliths. *Geochim. Cosmochim. Acta* **71**, 2736–2744.

Goreau T. F. (1959) The physiology of skeleton formation in corals. I. A method for measuring the rate of calcium deposition by corals under different conditions. *Biol. Bull.* **116**, 59–75.

Griffin S. and Druffel E. R. M. (1989) Sources of carbon to deep-sea corals. *Radiocarbon* **31**, 533–543.

Grossman E. L. and Ku T. L. (1986) Oxygen and carbon isotope fractionation in biogenic aragonite: temperature effects. *Chem. Geol.* **59**, 59–74.

Grottoli A. G. and Eakin C. M. (2007) A review of modern coral $\delta^{18}O$ and $\Delta^{14}C$ proxy records. *Earth Sci. Rev.* **81**, 67–91.

Guo W. (2008) Carbonate clumped isotope thermometre: application to carbonaceaous chondrites and effects of kinetic isotope fractionation. Ph. D. thesis, California Institute of Technology.

Guo W., Kim S., Thiagarajan N., Adkins J. F. and Eiler J. M. (2009) Mechanisms for "vital effects" in biogenic carbonates: new perspectives based on abundances of ^{13}C–^{18}O bonds. *Eos Trans. AGU* **90** (52) Fall Meet. Suppl. PP34B-07 (abstr.).

Holcomb M., Cohen A. L., Gabitov R. I. and Hutter J. L. (2009) Compositional and morphological features of aragonite precipitated experimentally from seawater and biogenically by corals. *Geochim. Cosmochim. Acta* **73**, 4166–4179.

Holcomb M., McCorkle D. C. and Cohen A. L. (2010) Long-term effects of nutrient and CO_2 enrichment on the temperate coral *Astrangia poculata* (Ellis and Solander, 1786). *J. Exp. Mar. Biol. Ecol.* **386**, 27–33.

Huntington K. W., Eiler J. M. E., Affek H. P., Guo W., Bonifacie M., Yeung L. Y., Thiagarajan N., Passey B., Tripati A., Daeron M. and Came R. (2009) Methods and limitations of 'clumped' CO2 isotope (Δ47) analysis by gas-source isotope ratio mass spectrometry. *J. Mass Spectrom.* **44**, 1318–1329.

Ingalls A. E., Lee C. and Druffel E. R. M. (2003) Preservation of organic matter in mound-forming coral skeletons. *Geochim. Cosmochim. Acta* **67**, 2827–2841.

Ip Y. K., Lim A. L. L. and Lim R. W. L. (1991) Some properties of calcium-activated adenosine triphosphatase from the hermatypic coral *Galaxea fascicularis*. *Mar. Biol.* **111**, 191–197.

Jacques T. G. and Pilson M. E. Q. (1980) Experimental ecology of the temperate scleractinian coral *Astrangia danae* I. Partition of respiration, photosynthesis and calcification between host and symbionts. *Mar. Biol.* **60**, 167–178.

Jacques T. G., Marshall N. and Pilson M. E. Q. (1983) Experimental ecology of the temperate scleractinian coral *Astrangia danae* II. Effect of temperature, light intensity and symbiosis with zooxanthellae on metabolic rate and calcification. *Mar. Biol.* **76**, 135–148.

Jones R. J., Hoegh-Guldberg O., Larkum A. W. D. and Schreiber U. (1998) Temperature-induced bleaching of corals begins with impairment of the CO2 fixation mechanism in zooxanthellae. *Plant Cell Environ.* **21**, 1219–1230.

Julliet-Leclerc A., Reynaud S., Rollion-Bard C., Cuif J. P., Dauphin Y., Blamart D., Ferrier-Pages C. and Allemand D. (2009) Oxygen isotopic signature of the skeletal microstructures in cultured corals: identification of vital effects. *Geochim. Cosmochim. Acta* **73**, 5320–5332.

Kilada R. W., Campana S. E. and Roddick D. (2007) Validated age, growth, and mortality estimates of the ocean quahog (*Arctica islandica*) in the western Atlantic. *ICES J. Mar. Sci.. J. Conseil* **64**, 31–38.

Kim S.-T. and O'Neil J. R. (1997) Equilibrium and nonequilibrium oxygen isotope effects in synthetic carbonates. *Geochim. Cosmochim. Acta* **61**, 3461–3475.

Kim S.-T., Hillaire-Marcel C. and Mucci A. (2006) Mechanisms of equilibrium and kinetic oxygen isotope effects in synthetic aragonite at 25 °C. *Geochim. Cosmochim. Acta* **70**, 5790–5801.

Kim S.-T., O'Neil J. R., Hillaire-Marcel C. and Mucci A. (2007a) Oxygen isotope fractionation between synthetic aragonite and water: influence of temperature and Mg^{2+} concentration. *Geochim. Cosmochim. Acta* **71**, 4704–4715.

Kim S.-T., Mucci A. and Taylor B. E. (2007b) Phosphoric acid fractionation factors for calcite and aragonite between 25 and 75 °C: revisited. *Chem. Geol.* **246**, 135–146.

Kluge T. and Affek H. P. (2012) Quantifying kinetic fractionation in Bunker Cave speleothems using Δ_{47}. *Quatern. Sci. Rev.* **49**, 82–94.

Land L. S., Lang J. C. and Barnes D. J. (1975) Extension rate: a primary control on the isotopic composition of West Indian (Jamaican) scleractinian reef coral skeletons. *Mar. Biol.* **3**, 221–233.

Lea D. W., Martin P. A., Chan D. A. and Spero H. J. (1995) Calcium uptake and calcification rate in the planktonic foraminifer *Orbulina universa*. *J. Foraminiferal Res.* **25**, 14–23.

Leder J. J., Swart P. K., Szmant A. M. and Dodge R. E. (1996) The origin of variations in the isotopic record of scleractinian corals: I. Oxygen. *Geochim. Cosmochim. Acta* **60**, 2857–2870.

Li H., Stott L. D. and Hammond D. E. (1997) Temperature and salinity effects on ^{18}O fractionation for rapidly precipitated carbonates: laboratory experiments with alkaline lake water. *Episode* **20**, 193–198.

Linsley B. K., Dunbar R. B., Wellington G. M. and Mucciarone D. A. (1994) A coral-based reconstruction of Intertropical Convergence Zone variability over Central America since 1707. *J. Geophys. Res.* **99**, 9977–9994.

Lough J. M. (2004) A strategy to improve the contribution of coral data to high-resolution paleoclimatology. *Palaeogeogr. Palaeoclimatol. Palaeoecol.* **204**, 115–143.

Lough J. M. (2008) Coral calcification from skeletal records revisited. *Mar. Ecol. Prog. Ser.* **373**, 257–264.

Lough J. M. and Barnes D. J. (1997) Several centuries of variation in skeletal extension, density and calcification in massive *Porites* colonies from the Great Barrier Reef: a proxy for seawater temperature and a background of variability against which to identify unnatural change. *J. Exp. Mar. Biol. Ecol.* **211**, 29–67.

Marshall A. T. (1996) Calcification in hermatypic and ahermatypic corals. *Science* **271**, 637–639.

McConnaughey T. (1989a) ^{13}C and ^{18}O isotopic disequilibrium in biological carbonates: I. Patterns. *Geochim. Cosmochim. Acta* **53**, 151–162.

McConnaughey T. (1989b) ^{13}C and ^{18}O isotopic disequilibrium in biological carbonates: II. In vitro simulation of kinetic isotope effects. *Geochim. Cosmochim. Acta* **53**, 163–171.

McConnaughey T. A. (2003) Sub-equilibrium oxygen-18 and carbon-13 levels in biological carbonates: carbonate and kinetic models. *Coral Reefs* **22**, 316–327.

McCrea J. M. (1950) On the isotopic chemistry of carbonates and a paleotemperature scale. *J. Chem. Phys.* **18**, 849–857.

Mills G. A. and Urey H. C. (1940) The kinetics of isotopic exchange between carbon dioxide, bicarbonate ion, carbonate ion and water. *J. Am. Chem. Soc.* **62**, 1019–1026.

Morcos S. A. (1970) Physical and chemical oceanography of the Red Sea. *Oceanogr. Mar. Biol. Annu. Rev.* **8**, 73–202.

Moya A., Tambutté S., Bertucci A., Tambutté E., Lotto S., Vullo D., Supuran C. T., Allemand D. and Zoccola D. (2008) Carbonic anhydrase in the scleractinian coral *Stylophora pistillata*: characterization, localization, and role in biomineralization. *J. Biol. Chem.* **283**, 25475–25484.

O'Leary M. H., Madhavan S. and Paneth P. (1992) Physical and chemical basis of carbon isotope fractionation in plants. *Plant, Cell Environ.* **15**, 1099–1104.

Omata T., Suzuki A., Sato T., Minoshima K., Nomaru E., Murakami A., Murayama S., Kawahata H. and Maruyama T. (2008) Effect of photosynthetic light dosage on carbon isotope composition in the coral skeleton: long-term culture of *Porites* spp.. *J. Geophys. Res.* **113**, G02014.

Passey B. H., Levin N. E., Cerling T. E., Brown F. H. and Eiler J. M. (2010) High-temperature environments of human evolution in East Africa based on bond ordering in paleosol carbonates. *Proc. Nat. Acad. Sci.* **107**, 11245–11249.

Pierrot D., Lewis E. and Wallace D. W. R. (2006) MS Excel program developed for CO_2 system calculations. ORNL/CDIAC-105a. Carbon Dioxide Information Analysis Center, Oak Ridge National Laboratory, US Department of Energy.

Quinn T. M., Crowley T. J., Taylor F. W., Henin C., Joannot P. and Join Y. (1998) A multicentury stable isotope record from a New Caledonia coral: interannual and decadal sea surface temperature variability in the southwest Pacific since 1657 A.D. *Paleoceanography* **13**, 412–426.

Reynolds R. W., Rayner N. A., Smith T. M., Stokes D. C. and Wang W. (2002) An improved in situ and satellite SST analysis for climate. *J. Clim.* **15**, 1609–1625.

Rollion-Bard C., Chaussidon M. and France-Lanord C. (2003) PH control on oxygen isotopic composition of symbiotic corals. *Earth Planet. Sci. Lett.* **215**, 275–288.

Rollion-Bard C., Chaussidon M. and France-Lanord C. (2011) Biological control of internal pH in scleractinian corals: Implications on paleo-pH and paleo-temperature reconstructions. *Comptes Rendus Geoscience* **343**, 397–405.

Romanek C., Grossman E. L. and Morse J. W. (1992) Carbon isotopic fractionation in synthetic aragonite and calcite: effects of temperature and precipitation rate. *Geochim. Cosmochim. Acta* **56**, 419–430.

Saenger C., Cohen A. L., Oppo D. W., Halley R. B. and Carilli J. E. (2009) Surface-temperature trends and variability in the low-latitude North Atlantic since 1552. *Nat. Geosci.* **2**, 492–495.

Schauble E. A., Ghosh P. and Eiler J. M. (2006) Preferential formation of ^{13}C–^{18}O bonds in carbonate minerals, estimated using first-principles lattice dynamics. *Geochim. Cosmochim. Acta* **70**, 2510–2529.

Schmid T., 2011. Clumped isotopes – a new tool for old questions: case studies on biogenic and inorganic carbonates. Ph. D. thesis, Eidgenössische Technische Hochschule (ETH), Zürich.

Schmid T. W. and Bernasconi S. M. (2010) An automated method for "clumped-isotope" measurements on small carbonate samples. *Rapid Commun. Mass Spectrom.* **24**, 1955–1963.

Shackleton N. (1967) Oxygen isotope analyses and Pleistocene temperatures re-assessed. *Nature* **215**, 15–17.

Siegenthaler U. and Münnich K. O. (1981) $^{13}C/^{12}C$ fractionation during CO_2 transfer from air to sea. In *Carbon Cycle Modelling* (ed. B. Bolin). John Wiley, New York.

Silverman D. N. (1982) Carbonic anhydrase: oxygen-18 exchange catalyzed by an enzyme with rate-contributing proton-transfer steps. *Methods Enzymol.* **87**, 732–752.

Smith J. E., Risk M. J., Schwarcz H. P. and McConnaughey T. A. (1997) Rapid climate change in the North Atlantic during the Younger Dryas recorded by deep-sea corals. *Nature* **386**, 818–820.

Spero H. J. and Lea D. W. (1996) Experimental determination of stable isotope variability in *Globigerina bulloides*: implications for paleoceanographic reconstructions. *Mar. Micropaleontol.* **28**, 231–246.

Spero H. J., Bijma J., Lea D. W. and Bemis B. E. (1997) Effect of seawater carbonate concentration on foraminiferal carbon and oxygen isotopes. *Nature* **390**, 497–500.

Squires D. F. (1960) Scleractinian corals from the Norfolk Island cable. *Rec. Auckland Inst. Museum* **5**, 195–201.

Tarutani T., Clayton R. N. and Mayeda T. K. (1969) The effect of polymorphism and magnesium substitution on oxygen isotope fractionation between calcium carbonate and water. *Geochim. Cosmochim. Acta* **33**, 987–996.

Thresher R. E., Tilbrook B., Fallon S., Wilson N. C. and Adkins J. (2011) Effects of chronic low carbonate saturation levels on the distribution, growth and skeletal chemistry of deep-sea corals and other seamount megabenthos. *Mar. Ecol. Prog. Ser.* **442**, 87–99.

Thiagarajan N., Adkins J. and Eiler J. (2011) Carbonate clumped isotope thermometry of deep-sea corals and implications for vital effects. *Geochim. Cosmochim. Acta* **75**, 4416–4425.

Tripati A. K., Eagle R. A., Thiagarajan N., Gagnon A. C., Bauch H., Halloran P. R. and Eiler J. M. (2010) ^{13}C–^{18}O isotope signatures and 'clumped isotope' thermometry in foraminifera and coccoliths. *Geochim. Cosmochim. Acta* **74**, 5697–5717.

Uchikawa J. and Zeebe R. E. (2012) The effect of carbonic anhydrase on the kinetics and equilibrium of the oxygen isotope exchange in the CO_2-H_2O system: implications on δ18 vital effects in biogenic carbonates. *Geochim. Cosmochim. Acta* **95**, 15–35.

Urey H. C., Lowenstam H. A., Epstein S. and McKinney C. R. (1951) Measurement of Paleotemperatures and temperatures of the upper Cretaceous of England, Denmark, and the southeastern United States. *Bulletin of the Geological Society of America* **62**, 399–416.

Usdowski E., Michaelis J., Böttcher M. E. and Hoefs J. (1991) Factors for the oxygen isotope equilibrium fractionation between aqueous and gaseous CO2, carbonic acid, bicarbonate, carbonate, and water (19°C). *Z. Phys. Chem.* **170**, 237–249.

Venn A., Tambutté E., Holcomb M., Allemand D. and Tambutté (2011) Live tissue imaging shows reef corals elevate pH under their calcifying tissue relative to seawater. *PLoS ONE* **6**, e20013.

Wang Z., Schauble E. A. and Eiler J. M. (2004) Equilibriumthermodynamics of multiply substituted isotopologues of molecular gases. *Geochim. Cosmochim. Acta* **68**, 4779–4797.

Watson E. B. (2004) A conceptual model for near-surface kinetic controls on the trace-element and stable isotope composition of abiogenic calcite crystals. *Geochimica et Cosmochimca Acta* **68**, 1473–1488.

Weber J. N. (1973) Deep-sea ahermatypic scleractinian corals: isotopic composition of the skeleton. *Deep Sea Res. Oceanogr. Abstr.* **20**, 901–909.

Weber J. N. and Woodhead P. M. J. (1972) Temperature dependence of oxygen-18 concentration in reef coral carbonates. *J. Geophys. Res.* **77**, 463–473.

Zaarur S., Olack G. and Affek H. P. (2011) Paleo-environmental implication of clumped isotopes in land snail shells. *Geochim. Cosmochim. Acta* **75**, 6859–6869.

Zeebe R. E. (1999) An explanation of the effect of seawater carbonate concentration on foraminiferal oxygen isotopes. *Geochim. Cosmochim. Acta* **63**, 2001–2007.

Zeebe R. E. (2007) An expression for the overall oxygen isotope fractionation between the sum of dissolved inorganic carbon and water. *Geochem. Geophys. Geosyst.* **8**, Q09002.

Zeebe R. E. and Wolf-Gladrow D. (2001) *CO_2 in Seawater: Equilibrium, Kinetics, Isotopes*. Elsevier Oceanography Series, 65, Amsterdam, p. 346.

Associate Editor: Claire Rollion-Bard